ARTICLE

CDK4/6 regulate lysosome biogenesis through TFEB/TFE3

Qiuyuan Yin[1]*, Youli Jian[2]* ![ORCID], Meng Xu[2] ![ORCID], Xiahe Huang[2], Niya Wang[3], Zhifang Liu[1], Qian Li[1], Jinglin Li[1], Hejiang Zhou[1], Lin Xu[3], Yingchun Wang[2], and Chonglin Yang[1] ![ORCID]

Lysosomes are degradation and signaling organelles that adapt their biogenesis to meet many different cellular demands; however, it is unknown how lysosomes change their numbers for cell division. Here, we report that the cyclin-dependent kinases CDK4/6 regulate lysosome biogenesis during the cell cycle. Chemical or genetic inactivation of CDK4/6 increases lysosomal numbers by activating the lysosome and autophagy transcription factors TFEB and TFE3. CDK4/6 interact with and phosphorylate TFEB/TFE3 in the nucleus, thereby inactivating them by promoting their shuttling to the cytoplasm. During the cell cycle, lysosome numbers increase in S and G2/M phases when cyclin D turnover diminishes CDK4/6 activity. These findings not only uncover the molecular events that direct the nuclear export of TFEB/TFE3, but also suggest a mechanism that controls lysosome biogenesis in the cell cycle. CDK4/6 inhibitors promote autophagy and lysosome-dependent degradation, which has important implications for the therapy of cancer and lysosome-related disorders.

Introduction

Lysosomes are the major digestive organelles that degrade both extra- and intracellular materials generated by endocytosis, phagocytosis, and autophagy; thus, they play important roles in many physiological processes such as the immune response, plasma membrane repair, bone resorption, and cell death (Luzio et al., 2007; Saftig and Klumperman, 2009; Xu and Ren, 2015; Yang and Wang, 2017). Lysosomes also serve as signaling hubs that sense cellular energy and amino acid levels and mediate signal transduction (Efeyan et al., 2015; Ferguson, 2015; Settembre et al., 2013). Because of their essential roles in cell homeostasis, the biogenesis and functions of lysosomes are tightly regulated. This is mainly achieved by regulating the subcellular localization and activities of TFEB and TFE3, two transcription factors of lysosome biogenesis and autophagy (Martina et al., 2014; Mills and Taghert, 2012; Raben and Puertollano, 2016; Sardiello et al., 2009; Settembre et al., 2011). For example, in cells with sufficient nutrients, the lysosome-localized mammalian target of rapamycin (mTOR) phosphorylates TFEB (at Ser142 and Ser211) and TFE3 (at Ser321), leading to their release from lysosomes and subsequent interaction with 14–3–3 proteins (Martina et al., 2012, 2014; Martina and Puertollano, 2013; Roczniak-Ferguson et al., 2012; Settembre et al., 2012). This keeps TFEB and TFE3 in the cytosol, where they are inactive.

When mTOR activity is inhibited by starvation or other conditions, no further phosphorylation of TFEB/TFE3 occurs; instead, they are dephosphorylated by the phosphatase calcineurin, leading to their nuclear translocation and activation (Medina et al., 2015; Wang et al., 2015). Other signals may converge on mTOR to regulate TFEB/TFE3 activity (Puertollano et al., 2018). In addition, PKC-GSK3β signaling regulates TFEB phosphorylation at Ser138 and Ser134 to affect its subcellular localization in an mTOR-independent manner (Li et al., 2016). More recently, it was found that the export of TFEB/TFE3 from the nucleus is mediated by the nuclear exportin CRM1 (Li et al., 2018; Napolitano et al., 2018). However, the signaling mechanism that directs TFEB/TFE3 nuclear export is unclear.

Although lysosomes are known to respond to many different signals by controlling their own biogenesis through TFEB and TFE3 (Raben and Puertollano, 2016; Settembre et al., 2013), it is not known whether lysosomes change their numbers in a mother cell for dispensation to daughter cells at mitotic cell division. Successful cell division involves G1 (the first gap), S (DNA synthesis), G2 (the second gap), and M (mitosis) phases, which are driven by cyclin-dependent kinases (CDKs; Asghar et al., 2015; Lim and Kaldis, 2013; Sherr et al., 2016); however, the link between cell cycle progression and lysosome biogenesis

remains to be uncovered. Here, we reveal the essential role of CDK4 and CDK6 in the nuclear export of TFEB and TFE3. We found that CDK4 and CDK6 interact with and phosphorylate nuclear TFEB and TFE3, thereby promoting their shuttling to the cytoplasm. We further found that lysosome biogenesis is elevated at the S and G2/M phases when the levels of cyclin D1, the activator of CDK4 and CDK6, decline. These results thus reveal not only a mechanism that directs the nuclear export of TFEB and TFE3 but also a mechanism that regulates lysosome biogenesis in the cell cycle.

Results

CDK4/6 inhibitors induce TFEB- and TFE3-dependent lysosome biogenesis

To explore the mechanisms that underlie lysosome biogenesis, we performed screens for both natural and commercial small-molecule compounds that increase lysosomal abundance. We previously reported that the natural compounds HEP14 and HEP15 induce lysosome biogenesis in an mTOR-independent and PKC-dependent manner (Li et al., 2016). Our screen also identified two commercial compounds, LY2835219 (abemaciclib) and PD0332991 (palbociclib), that are known to specifically inhibit CDK4/6 (Fig. 1 A and Table S1). Both LY2835219 and PD0332991 increased LysoTracker Red staining in HeLa cells in a concentration-dependent manner, similar to the mTOR inhibitor Torin 1 (Fig. 1, A and B). LY2835219 also increased Lyso-Tracker Red staining in several other cell types (Fig. S1 A). Western blotting and immunostaining indicated that the protein levels of lysosome-associated membrane protein l (LAMP1) and lysosome-integral membrane protein II (LIMPII) were significantly increased following LY2835219 treatment (Fig. 1, C and D). Lysosome numbers, measured by counting LAMP1 foci, were also significantly elevated (Fig. 1 D). In addition, LY2835219 triggered the formation of GFP-LC3 puncta (Fig. 1 E), and the endogenous levels of LC3B-II were strongly increased (Fig. 1, E and F). PD0332991 enhanced endogenous LAMP1 levels and LC3B puncta, like Torin 1 (Fig. S1 B). Using RFP-GFP-LC3 as an indicator, we confirmed that LY2835219 strongly induced the formation of autolysosomes (foci positive for RFP and negative for GFP; Fig. S1 C). Coimmunostaining of endogenous LAMP1 with mCherry in mCherry-LC3–expressing cells further revealed that the numbers of both free lysosomes (foci positive for LAMP1 and negative for mCherry-LC3) and autolysosomes (foci positive for both LAMP1 and mCherry-LC3) were significantly increased by LY2835219 (Fig. S1 D). Collectively, the above findings suggest that these CDK4/6 inhibitors induced lysosome biogenesis and autophagy.

We next investigated if the ability of the CDK4/6 inhibitors to increase lysosome abundance requires TFEB and TFE3, the transcription factors that scale lysosome biogenesis and autophagy (Mills and Taghert, 2012; Raben and Puertollano, 2016; Settembre et al., 2013). siRNA depletion of both TFEB and TFE3 significantly reduced the LY2835219- and Torin 1–induced increases in LAMP1 and LC3B, as indicated by immunostaining (Fig. 1, G and H). This suggests that these CDK4/6 inhibitors, like Torin 1, function through TFEB and TFE3 to induce lysosome

biogenesis. Supporting this conclusion, LY2835219 and PD0332991 treatment led to obvious nuclear localization of endogenous TFEB and TFE3, as well as ectopically expressed TFEB-EGFP, mCherry-TFE3, and EGFP-TFE3 (Fig. 1 I and Fig. S1 E). Consistent with this, several TFEB/TFE3 target genes were significantly up-regulated following exposure of cells to LY2835219 (Fig. S1 F; Sardiello et al., 2009). Pharmacological inhibitors of other CDKs—except for R547 and SU9516, which are weakly active against CDK4—did not induce obvious nuclear translocation of TFEB-EGFP (Table S1). These results indicate that specific inhibition of CDK4/6 leads to TFEB and TFE3 activation and consequently to increased lysosome biogenesis and autophagy.

Genetic depletion of CDK4 or CDK6 leads to TFEB and TFE3 activation

To consolidate the conclusion that CDK4/6 inhibition led to TFEB/TFE3 activation and lysosome biogenesis, we knocked down both CDK4 and CDK6 in HeLa cells using siRNA. CDK4/6 knockdown strongly increased LysoTracker Red staining, LAMP1 protein levels, and the number of LAMP1 foci, as revealed by immunostaining and Western blotting (Fig. 2, A and B). To corroborate these results, we further generated CDK4 knockout (KO) and CDK6 KO HeLa cells using CRISPR/Cas9. Cells with KO of CDK4 or CDK6 had strongly increased Lyso-Tracker Red staining, LAMP1 levels, and numbers of LAMP1 foci compared with the control HeLa cells (Fig. 2, C and D). In addition, LC3 puncta and LC3B-II levels were also significantly increased in these KO cells compared with the control (Fig. 2, E and F). These results suggest that loss of CDK4 or CDK6 led to lysosome biogenesis and autophagy.

We then examined the subcellular localizations of TFEB and TFE3. Compared with control cells, a higher percentage of CDK4 KO and CDK6 KO cells had nucleus-localized endogenous TFEB and TFE3 (Fig. 2 G). Similarly, ectopically expressed TFEB-EGFP and EGFP-TFE3 also localized to the nucleus in a high percentage of CDK4 and CDK6 KO cells compared with their predominantly cytosolic localization in control cells (Fig. 2 G). LY2835219 further increased the nuclear localization of endogenous TFEB and TFE3 in CDK4 KO cells and CDK6 KO cells (Fig. S1 G), which suggests that CDK4 and CDK6 probably act redundantly on these transcription factors. siRNA knockdown of TFEB and TFE3 significantly suppressed the increase in LAMP1 levels, LAMP1 foci, and LC3 puncta in CDK4 KO cells and CDK6 KO cells (Fig. 2, H and I). Taken together, these findings confirmed that inhibition or loss of CDK4/6 led to TFEB and TFE3 activation, and hence, lysosome biogenesis and autophagy.

CDK4 and CDK6 interact with TFEB and TFE3 in the nucleus

We next investigated how CDK4 and CDK6 activate TFEB and TFE3. In HeLa cells, LY2835219 treatment did not obviously change the phosphorylation of the mTOR substrates S6 kinase or ULK1, in contrast to the strong inhibition of phosphorylation by Torin 1 (Fig. S2 A). Similarly, LY2835219 did not change the phosphorylation of ERK1/2 (extracellular regulated protein kinase 1/2) or AKT, in contrast to the inhibitors of these kinases (Fig. S2, B and C). In addition, LY2835219 did not change GSK3β
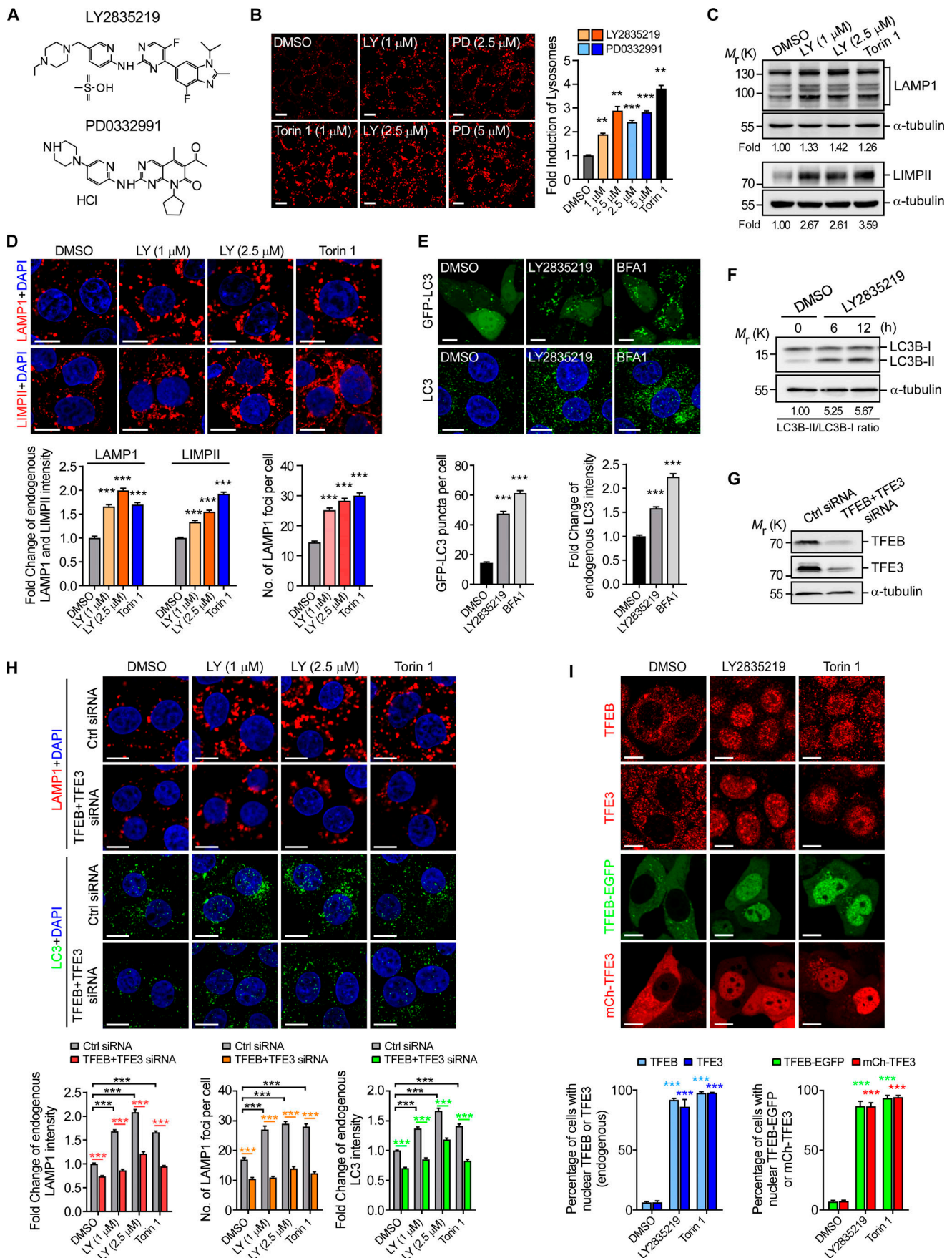
Yin et al.
Lysosome biogenesis in the cell cycle

Journal of Cell Biology 3 of 20
https://doi.org/10.1083/jcb.201911036

phosphorylation or induce membrane translocation of PKCα or PKCδ, unlike HEP14 (Li et al., 2016; Fig. S2, D and E), which indicates that CDK4/6 inhibition did not affect the PKC-GSK3β signaling axis. Consistent with these findings, phosphorylation of ULK1, ERK1/2, and GSK3β was not changed in CDK4 or CDK6 KO cells (Fig. S2 F). CDK4 or CDK6 KO did not change the subcellular localization of either PKCα or PKCδ (Fig. S2 G). Thus, inhibition of CDK4/6 did not cause TFEB/TFE3 activation by directly affecting mTOR, ERK1/2, AKT, GSK3β, or PKC.

We thus investigated if CDK4 and CDK6 directly act on TFEB and TFE3. In cells under normal conditions, immunostaining assays revealed that CDK4 and CDK6 and their cofactors cyclin D1 and cyclin D3 predominantly localized to the nucleus, while TFEB-EGFP and EGFP-TFE3 were cytosolic (Fig. 3, A–D; and Fig. S3, A–D). When cells were treated with Torin 1, TFEB-EGFP and EGFP-TFE3 translocated into the nucleus and showed increased colocalization with CDK4 and CDK6, as well as with cyclin D1 and cyclin D3 (Fig. 3, A–D; and Fig. S3, A–D). Using coimmunoprecipitation (Co-IP) assays, we found that ectopically expressed EGFP-CDK4 and EGFP-CDK6 were coprecipitated with Flag-TFEB and Flag-TFE3 (Fig. 3, E and F). Similarly, ectopically expressed cyclin D1–EGFP and cyclin D3–EGFP interacted with Flag-TFEB and Flag-TFE3 in Co-IP assays (Fig. S3, E–H).

We next investigated where the interactions of TFEB and TFE3 with CDK4 and CDK6 occur. Subcellular fractionation indicated that endogenous TFEB and TFE3 are predominantly cytosolic, while CDK4, CDK6, cyclin D1, and cyclin D3 are enriched in the nucleus (Fig. 3 G). However, in Co-IP assays, cytosolic TFEB and TFE3 did not coprecipitate with cytosolic CDK4, CDK6, cyclin D1, or cyclin D3. In contrast, nuclear TFEB and TFE3 were coimmunoprecipitated with nuclear CDK4, CDK6, cyclin D1, and cyclin D3 (Fig. 3, H–K). Taken together, these results indicated that TFEB and TFE3 interact with CDK4 and CDK6 in the nucleus.

CDK4 and CDK6 phosphorylate TFEB and TFE3

We then investigated whether CDK4 and CDK6 phosphorylate TFEB and TFE3. We purified recombinant proteins of His6- and SMT-fused TFEB(1–130), TFEB(105–300), and TFEB(295–476)

and incubated them with recombinant CDK4/cyclin D1 or CDK6/cyclin D3 complex in the presence of ^{32}γ-ATP. Both CDK4 and CDK6 phosphorylated these TFEB fragments (Fig. 4 A). The strongest phosphorylation signals were observed in the reactions containing CDK4 + TFEB(295–476) and CDK6 + TFEB(105–300). The phosphorylation reactions were inhibited by LY2835219 (Fig. 4 A), indicating that the phosphorylation was dependent on CDK4/6.

We next performed mass spectrometry to determine which amino acid residues in these TFEB fragments were phosphorylated. Our results indicated that Ser114, Ser142, Thr331, and Ser467 were most frequently phosphorylated by both CDK4 and CDK6 (Fig. 4 B and Fig. S4). We thus mutated these residues individually in TFEB-EGFP and examined the subcellular localizations of the mutant proteins. Neither S114A nor T331A caused obvious nuclear localization of TFEB-EGFP; however, TFEB(S142A)–EGFP was observed in the nucleus in ~70% of cells (Fig. 4 C), as reported previously (Settembre et al., 2011, 2012). The S467A mutation also led TFEB-EGFP to localize to the nucleus in a substantial population of cells (Fig. 4 C), as reported (Palmieri et al., 2017). Nevertheless, TFEB-EGFP containing S114A/S142A/T331A/S467A had a similar nuclear distribution to the S142A mutant (Fig. 4 C). Thus, although CDK4 and CDK6 phosphorylate TFEB at multiple sites, the phosphorylation at Ser142 plays a major role in preventing TFEB from localizing to the nucleus. Supporting this notion, in vitro phosphorylation by CDK4 or CDK6 of TFEB(105–300) containing S142A, but not S211A, was strongly reduced compared with the WT (Fig. 4 D). In addition, LY2835219 strongly inhibited the phosphorylation of TFEB at Ser142 in cells expressing TFEB-EGFP, as detected with an antibody that recognizes phospho-Ser142 (p-Ser142) of TFEB, p-Ser246 of TFE3, and p-Ser180 of microphthalmia-associated transcription factor (MITF; Fig. 4 E). In CDK4 and CDK6 KO cells, the p-Ser142 signal was decreased compared with that in control HeLa cells (Fig. 4 F). Collectively, these findings indicate that CDK4/6 phosphorylate TFEB on Ser142 in cells.

Because TFE3 shares high similarity with TFEB (Fig. 4 G), we performed in vitro phosphorylation of recombinant TFE3(213–411), which contains Ser246, the residue corresponding to Ser142 in
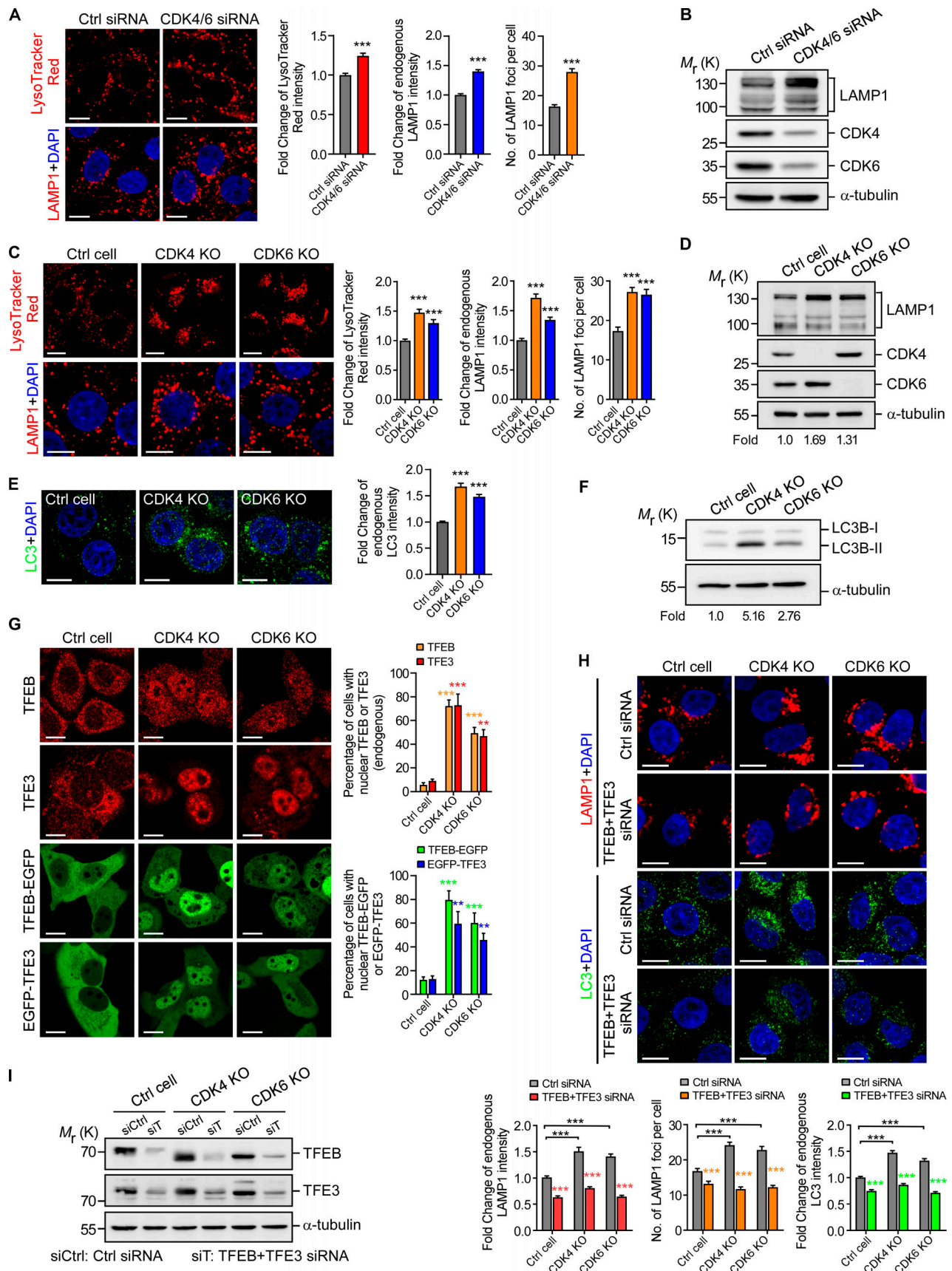
Figure 2. Genetic depletion of CDK4 and CDK6 leads to TFEB and TFE3 activation. (A) CDK4 and CDK6 knockdown induced lysosome biogenesis. Left: Images of LysoTracker Red staining and LAMP1 staining of HeLa cells treated with control siRNA (Ctrl siRNA) or siRNA of CDK4 and CDK6 (CDK4/6 siRNA).

Right: Quantification (fold changes of LysoTracker Red staining, endogenous LAMP1 immunostaining, and number of LAMP1 foci) of lysosomes in HeLa cells treated with Ctrl siRNA or CDK4/6 siRNA. ≥50 cells were quantified for each treatment. **(B)** Immunoblotting of LAMP1, CDK4, CDK6, and α-tubulin in HeLa cells treated with Ctrl siRNA or CDK4/6 siRNA. Cells were analyzed 48 h after transfection. **(C)** Lysosome biogenesis is increased in CDK4 KO and CDK6 KO cells. Left: Images of LysoTracker Red staining and endogenous LAMP1 immunostaining in Ctrl, CDK4 KO, and CDK6 KO cells. Right: Quantification (fold change) of LysoTracker Red staining, endogenous LAMP1 staining, and number of LAMP1 foci in Ctrl, CDK4, and CDK6 KO cells. Comparisons are between Ctrl and KO cells. ≥40 cells were quantified in each group. **(D)** Immunoblotting of LAMP1, CDK4, CDK6, and α-tubulin in Ctrl, CDK4 KO, and CDK6 KO cells. Fold induction of proteins was normalized by LAMP1/α-tubulin ratios. **(E)** Autophagy is increased in CDK4 KO and CDK6 KO cells. Left: Images of endogenous LC3B immunostaining in Ctrl, CDK4 KO, and CDK6 KO cells. Right: Quantification of endogenous LC3B immunostaining. Comparisons are between Ctrl and KO cells. ≥120 cells were quantified in each group. **(F)** Immunoblotting of LC3B-I and LC3B-II in Ctrl, CDK4 KO, and CDK6 KO cells. Fold induction of LC3B-II/LC3B-I was normalized by α-tubulin. **(G)** Left: Images of the subcellular localization of endogenous TFEB, endogenous TFE3, TFEB-EGFP, or EGFP-TFE3 in Ctrl, CDK4 KO, and CDK6 KO cells. Right: Quantification of nuclear localized endogenous TFEB and TFE3 or TFEB-EGFP and EGFP-TFE3 in Ctrl, CDK4 KO, and CDK6 KO cells. Comparisons are made between Ctrl and KO cells within the same color group. ≥500 cells were quantified in each group. **(H)** Images (upper) and quantification (lower) of lysosomes (fold change of endogenous LAMP1 immunostaining and number of LAMP1 foci) and autophagic level (fold change of endogenous LC3B immunostaining) in Ctrl, CDK4 KO, and CDK6 KO cells treated with Ctrl siRNA or TFEB+TFE3 siRNA. ≥40 cells were quantified for each treatment. **(I)** Immunoblotting of TFEB and TFE3 in Ctrl, CDK4 KO, and CDK6 KO cells treated with control siRNA (siCtrl) and TFEB+TFE3 siRNA (siT). Cells were subjected to Western blot analysis using TFEB and TFE3 antibody 48 h after transfection of siRNA oligos. Scale bars represent 10 μm in all images. For all quantifications, data (mean ± SEM) were from three independent experiments and were analyzed using the unpaired two-tailed t test or one-way ANOVA with the post hoc Holm-Sidak test. **, $P < 0.01$; ***, $P < 0.001$.

TFEB (Fig. 4 G). Both CDK4 and CDK6 phosphorylated TFE3(213–411) in an LY2835219-dependent manner (Fig. 4 H). When Ser246 was mutated to Ala, the phosphorylation signals were strongly reduced (Fig. 4 H). Using the same antibody that recognizes p-Ser142 in TFEB, which also recognizes p-Ser246, we found that LY2835219 strongly inhibited EGFP-TFE3 phosphorylation at Ser246 in cells (Fig. 4 I). The p-Ser246 signals were also decreased in CDK4 or CDK6 KO cells (Fig. 4 J). Consistent with this, EGFP-TFE3(S246A) strongly localized to the nucleus (Fig. 4 K). The TFE3(S568A) mutation, like TFEB(S467A), increased the degree of nuclear localization (Fig. 4 K). However, the TFE3 S246A/S568A double mutation did not significantly increase the nuclear localization compared with the S246A single mutation (Fig. 4 K), which suggests that Ser246 is the determinant for TFE3 to localize to the nucleus. Altogether, these results suggest that TFE3 phosphorylation at Ser246 by CDK4/6, like TFEB phosphorylation at Ser142, prevents it from localizing to the nucleus.

Phosphorylation of TFEB and TFE3 by CDK4/6 is essential for their nuclear export

TFEB and TFE3 shuttle between the cytosol and lysosomes and between the cytosol and the nucleus (Napolitano et al., 2018; Raben and Puertollano, 2016). Under normal conditions, TFEB and TFE3 imported into the nucleus probably move quickly back to the cytosol, and thus they are mainly observed in the cytosol. Supporting this notion, inactivation of the nuclear pore protein CRM1 causes nuclear retention of TFEB (Li et al., 2018; Napolitano et al., 2018). Because CDK4/6 mainly localize in the nucleus, where they interact with and phosphorylate TFEB and TFE3 (Fig. 3 and Fig. 4), we reasoned that they should play a role in the nuclear export of TFEB and TFE3. To test this hypothesis, we examined the effect of LY2835219 on the localization of TFEB and TFE3 in cells with hyperactive mTOR caused by ectopic expression of RagA$_{GTP}$-RagC$_{GDP}$ or RagB$_{GTP}$-RagD$_{GDP}$ (Martina et al., 2014; Martina and Puertollano, 2013). Whereas Torin 1, which inhibits mTOR directly, induced nuclear translocation of TFEB-EGFP and EGFP-TFE3 in cells expressing RagA$_{GTP}$-RagC$_{GDP}$ or RagB$_{GTP}$-RagD$_{GDP}$, LY2835219 failed to induce

nuclear localization of TFEB and TFE3 in the same cells (Fig. 5 A). These results suggest that CDK4/6 act on TFEB and TFE3 only after they enter the nucleus. Consistent with this, LY2835219 failed to inhibit phosphorylation of TFEB at Ser142 and of TFE3 at Ser246 (Fig. 5, B and C). In contrast, Torin 1 inhibited the phosphorylation of TFEB at Ser142 and of TFE3 at Ser246 in cells expressing RagA$_{GTP}$-RagC$_{GDP}$ or RagB$_{GTP}$-RagD$_{GDP}$ (Fig. 5, B and C). One explanation for this is that inhibition of mTOR not only directly suppressed mTOR-mediated phosphorylation of TFEB Ser142 and TFE3 Ser246 (Puertollano et al., 2018) but also suppressed CDK4/6 activities by down-regulating cyclin D (Alao, 2007). Importantly, the interaction of Flag-tagged TFEB(S142A) with EGFP-tagged CRM1, which is required for TFEB/TFE3 nuclear export (Li et al., 2018; Napolitano et al., 2018), was strongly reduced compared with Flag-tagged WT TFEB in Co-IP assays (Fig. 5 D). These findings, together with the fact that TFEB(S142A) and TFE3(S246A) localize to the nucleus (Fig. 4), suggest that CDK4/6 phosphorylate TFEB and TFE3 in the nucleus to promote their CRM1-dependant nuclear export.

To consolidate this conclusion, we treated HeLa cells expressing TFEB-EGFP or EGFP-TFE3 with Torin 1 to induce their nuclear translocation. We then removed Torin 1 and monitored their export from the nucleus over time. TFEB-EGFP and EGFP-TFE3 rapidly lost their nuclear localization following removal of Torin 1 (Fig. 5, E and F). For example, only ~20% of cells had obvious nuclear TFEB and TFE3 3 h after removal of Torin 1, compared with ~100% of cells at the starting time point (Fig. 5, E and F). In the presence of LY2835219, however, ~90% of cells still contained nuclear TFEB and TFE3 3 h after Torin 1 removal (Fig. 5, E and F). In CDK4 KO and CDK6 KO cells, nuclear export of TFEB-EGFP and EGFP-TFE3 induced by similar removal of Torin 1 was strongly inhibited (Fig. S5, A and B). These findings suggest that inhibition of CDK4/6 prevents TFEB and TFE3 from leaving the nucleus.

In addition, we examined fluorescence loss in photobleaching (FLIP) of the cytosolic TFEB-EGFP signals following removal of Torin 1. Continuous bleaching of cytosolic TFEB-EGFP led to a sharp decrease in nuclear TFEB-EGFP signals, indicating that nuclear TFEB-EGFP was exported from the nucleus to the
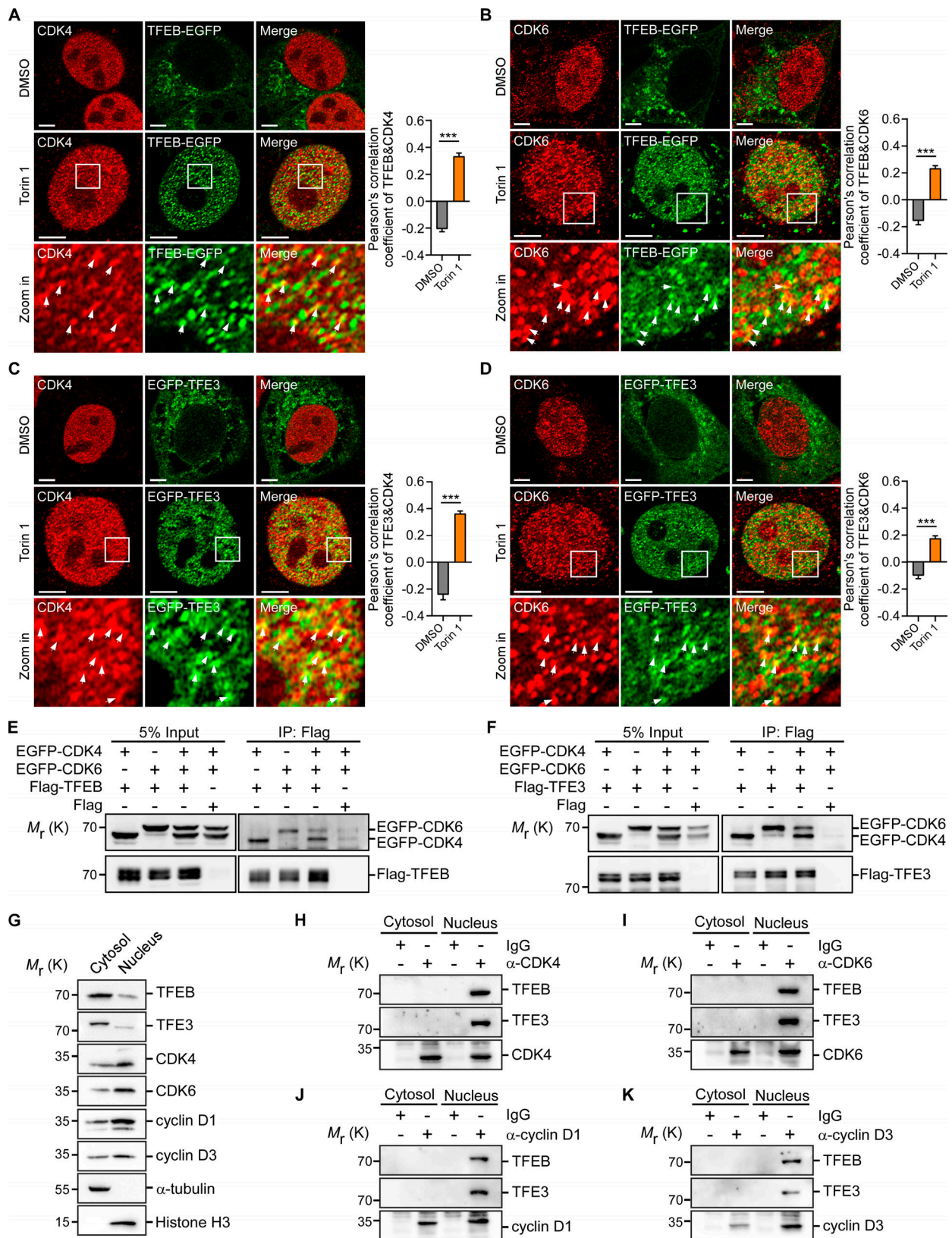
Figure 3. **CDK4 and CDK6 interact with TFEB and TFE3 in the nucleus. (A and B)** Colocalization of TFEB-EGFP with endogenous CDK4 (A) and CDK6 (B). HeLa cells transfected with TFEB-EGFP were treated with Torin 1 (1 µM, 3 h), fixed, and stained with CDK4 or CDK6 antibody. Framed regions in the middle row are magnified and shown at the bottom. Arrowheads indicate the colocalized proteins. Quantification of protein colocalization is shown in the right panels. **(C and D)** Colocalization of EGFP-TFE3 with CDK4 (C) and CDK6 (D). HeLa cells transfected with EGFP-TFE3 were treated with Torin 1 (1 µM, 3 h), fixed, and stained with CDK4 or CDK6 antibody. Framed regions in the middle row are magnified and shown at the bottom. Arrowheads indicate the colocalized proteins.

Quantification of protein colocalizations are shown on the right panels. **(E and F)** Co-IP of Flag-TFEB (E) or Flag-TFE3 (F) with EGFP-CDK4 and EGFP-CDK6. IPs were performed with Flag antibody, and precipitated proteins were detected with antibodies against Flag or GFP. **(G)** Immunoblotting of the indicated proteins in cytosolic and nuclear fractions. Nuclear and cytosolic fractions were prepared and subjected to Western blotting with the indicated antibodies. **(H–K)** Co-IPs of TFEB and TFE3 with CDK4 (H), CDK6 (I), cyclin D1 (J), and cyclin D3 (K) in nuclear and cytosolic fractions. IPs of endogenous CDK4, CDK6, cyclin D1, and cyclin D3 were performed with the respective antibodies. Precipitated proteins were detected with antibodies against the indicated proteins. Scale bars represent 5 µm in all images. For all quantifications, data (mean ± SEM) were from three independent experiments and were analyzed using the unpaired two-tailed *t* test. ≥30 cells were quantified for each treatment. ***, P < 0.001.

cytosol, where it was bleached (Fig. 5, G and H). In contrast, nuclear TFEB-EGFP signals decreased at a much slower rate in the same photobleaching assay in the presence of LY2835219 (Fig. 5, G and H).

To determine the specific effect of CDK4/6 on the nuclear export of TFEB and TFE3, we examined the subcellular localization of EGFP-tagged FOXO3 and nuclear factor κB (NF-κB), two transcription factors that undergo nucleo-cytoplasmic shuttling and require CRM1 for nuclear export (Latré de Laté et al., 2010; Zhang et al., 2012). Unlike TFEB-EGFP and EGFP-TFE3, FOXO3-EGFP and NF-κB–EGFP were cytosolic in CDK4 KO and CDK6 KO cells (Fig. S5 C). In addition, we treated HeLa cells expressing FOXO3-EGFP and NF-κB–EGFP with LY2835219 or the CRM1 inhibitor leptomycin B (LMB). While LMB caused strong nuclear retention of all four transcription factors, LY2835219 did not change the cytosolic localization of FOXO3 and NF-κB (Fig. S5 D). Altogether, these results demonstrate that CDK4/6 phosphorylate nuclear TFEB and TFE3 to recycle them back to the cytosol.

CDK4/6 regulate cell cycle–dependent lysosome biogenesis

The findings that CDK4/6 inhibition led to nuclear retention and activation of TFEB and TFE3 prompted us to examine lysosome biogenesis during the cell cycle. We simultaneously stained HeLa, HepG2, and HCT116 cells with Hoechst 33342, which labels chromosomal DNA, and LysoTracker Red, which stains lysosomes, and performed flow cytometry to analyze lysosomal abundance in each phase of the cell cycle. In all cell types examined, cells at the S and G2/M phases had a significantly higher intensity of LysoTracker Red staining than the G1 phase cells (Fig. 6, A and D). In another assay, we first fed cells with FITC-Dextran and allowed it to reach lysosomes, and then we fixed the cells and stained them with propidium iodide (PI), which labels nuclear DNA. We then performed flow cytometry to determine lysosome numbers in cells at distinct cell cycle phases. The results indicated that cells at the S and G2/M phases had a significantly higher intensity of FITC-Dextran labeling than cells at the G1 phase (Fig. 6, B and D). Furthermore, we immunostained endogenous LAMP1 in HeLa, HepG2, and HCT116 cells and performed flow cytometry. We found that LAMP1 staining was significantly increased in cells at the S and G2/M phases compared with cells at the G1 phase (Fig. 6, C and D). Collectively, these findings indicated that lysosome biogenesis is increased in the S and G2/M phases of the cell cycle.

CDK4 and CDK6 are known to drive G1 phase progression, and their activities are dependent on D-type cyclins (Fig. 6 E; Asghar et al., 2015; Lim and Kaldis, 2013; Sherr et al., 2016). Cyclin D1 is quickly degraded at the G1/S boundary of the cell cycle by the ubiquitin–26S proteasome pathway, thus switching

off CDK4/6 activities (Fig. 6 E; Alt et al., 2000; Diehl et al., 1998, 1997; Qie and Diehl, 2016; Sherr et al., 2016). To determine whether the increase in lysosome biogenesis corresponds to this inactivation of CDK4/6, we synchronized cells to distinct cell cycle stages using standard assays (Ma and Poon, 2011). In HeLa, HepG2, and HCT116 cells, the S, G2, and M phases had strongly increased LAMP1 levels compared with the G1 phase, while the cyclin D1 protein levels were greatly decreased (Fig. 6, F and G). The levels of cyclin E1, which activates CDK2 at the late G1 stage (Goel et al., 2018; Koff et al., 1992; Sherr et al., 2016), were also down-regulated like cyclin D1 (Fig. 6 G), as reported previously (Baldin et al., 1993; Koff et al., 1992). In contrast, cyclin B1, which activates CDK1 in the M phase (Goel et al., 2018; Lim and Kaldis, 2013; Sherr et al., 2016), was increased at the G2 and M phases (Fig. 6 G). Pharmacological inhibition of CDK1, CDK2, and other CDKs did not activate TFEB (Table S1), while CDK4/6 inhibition led to increased lysosome biogenesis in a TFEB- and TFE3-dependent manner. These findings collectively suggest that the CDK4/6–TFEB/TFE3 axis contributes to the elevated lysosome biogenesis at the S–M phases.

To further investigate the role of the CDK4/6–TFEB/TFE3 axis in lysosome biogenesis in the cell cycle, we first determined the lysosome abundance in CDK4 KO and CDK6 KO cells. Compared with the control cells at the G1 phase, CDK4 KO and CDK6 KO cells at G1 had significant increases in the intensity of LysoTracker Red staining (Fig. 7 A). This indicates that reducing CDK4/6 activity indeed led to elevated lysosome biogenesis. CDK4 KO and CDK6 KO cells at the S–M phases also had a higher intensity of LysoTracker Red staining, which likely resulted from a stronger effect of CDK4 or CDK6 KO compared with cyclin D turnover-induced decline in CDK4/6 activity in control cells at the S–M phases (Fig. 7 A).

We further treated HeLa cells with LY2835219 for 12 h, which more thoroughly inhibited CDK4/6 activity (Jansen et al., 2017), and examined lysosomal abundance in each cell cycle phase. LY2835219 significantly increased LysoTracker Red staining in G1 cells, and the increase was comparable with that in S and G2/M cells not treated with LY2835219 (Fig. 7 B). Thus, inhibition of CDK4/6 at G1 enhanced lysosome biogenesis, similar to the lysosomal increase at the S and G2/M phases when CDK4/6 activity was diminished by cyclin D turnover. Intriguingly, LY2835219 further enhanced LysoTracker Red staining in S and G2/M cells (Fig. 7 B). A possible explanation for this is that S–M–phase cells have residual CDK4/6 activities; thus, inhibition of CDK4/6 further increased lysosomal abundance.

We next performed siRNA to knock down TFEB and TFE3 together, and we analyzed lysosomal abundance in each phase of the cell cycle in HeLa cells. TFEB + TFE3 siRNA significantly reduced lysosomal abundance, measured with LysoTracker Red

Yin et al.
Lysosome biogenesis in the cell cycle

Journal of Cell Biology 8 of 20
https://doi.org/10.1083/jcb.201911036

A In vitro phosphorylation panels showing CDK4/cyclin D1 and CDK6/cyclin D3 with TFEB fragments 1-130, 105-300, 295-476 ± LY2835219, γ-³²P autoradiography and M_r (K) Coomassie.

B

CDK4/cyclin D1			
TFEB	Peptide	Site	PSMs
1-130	¹⁰³FAAHISPAQG**S**PKPPPAASPGVR¹²⁶	Ser114	5
105-300	¹²⁷AGHVLSSSAGNSAPN**S**PMAMLHIGSNPER¹⁵⁵	Ser142	4
295-476	⁴⁶⁵RS**S**FSMEEGDVL⁴⁷⁴	Ser467	6

CDK6/cyclin D3			
1-130	¹⁰³FAAHISPAQG**S**PKPPPAASPGVR¹²⁶	Ser114	4
105-300	¹²⁷AGHVLSSSAGNSAPN**S**PMAMLHIGSNPER¹⁵⁵	Ser142	15
295-476	³²⁵VHGLPTT**T**SPSGMNMAELAQQVVK³⁴⁷	Thr331	5
	⁴⁶⁵RS**S**FSMEEGDVL⁴⁷⁴	Ser467	5

Red: Phosphorylation   PSMs: Peptide Spectrum Matches

Figure 4. **CDK4 and CDK6 phosphorylate TFEB and TFE3. (A)** In vitro phosphorylation of His6-SMT3-fused TFEB(1–130), TFEB(105–300), and TFEB(295–476) by CDK4/cyclin D1 complex or CDK6/cyclin D3 complex. Phosphorylated proteins were detected by autoradiography (upper panels). The same gel was stained with Coomassie blue to visualize the total proteins (lower panels). **(B)** Mass spectrometry–based identification of TFEB peptides with amino acid residues phosphorylated by CDK4/cyclin D1 and CDK6/cyclin D3. Phosphorylation sites identified by mass spectrometry are indicated in red. Peptide

spectrum matches (PSMs) indicate the total number of peptides identified. **(C)** Images (upper) and quantification (lower) of the ratio of nucleus-localized WT TFEB-EGFP and mutant TFEB-EGFP: S114A, S142A, T331A, S467A, S114A/T331A/S467A, S142A/S467A, and S114A/S142A/T331A/S467A. For quantification, comparisons are between WT and mutant TFEB except for the datasets linked by lines. **(D)** In vitro phosphorylation of WT and mutant His6-SMT3-TFEB(105–300) by CDK4/cyclin D1 complex and CDK6/cyclin D3 complex. Phosphorylated proteins were detected by autoradiography (upper panels), and the same gel was stained with Coomassie blue to visualize the total proteins (lower panels). Relative fold change of TFEB phosphorylation in each mutant was normalized by total proteins. LY, LY2835219. **(E)** LY2835219 strongly reduces the Ser142 phosphorylation in TFEB. HeLa cells expressing TFEB-EGFP were treated with LY2835219 (1 µM, 2.5 µM, 3 h) and immunoprecipitated with GFP-Trap beads. The precipitated proteins were detected with antibodies against phospho-[TFEB(Ser142)/TFE3(Ser246)/MITF(Ser180)] (upper) and EGFP (lower). Relative fold change of phospho-TFEB(Ser142) was normalized by EGFP intensity. **(F)** Phosphorylation of Ser142 in TFEB is decreased in CDK4 or CDK6 KO cells. Control (Ctrl), CDK4 KO, and CDK6 KO cells were transfected with TFEB-EGFP for 24 h and immunoprecipitated with GFP-Trap beads. The precipitated proteins were detected with antibodies against phospho-[TFEB(Ser142)/TFE3(Ser246)/MITF(Ser180)] (upper), EGFP, CDK4, and CDK6. Relative fold change of phospho-TFEB(Ser142) is normalized by EGFP intensity. **(G)** Schematic comparison of the protein structures of TFEB and TFE3 (top) and the amino acid sequence around the key phosphorylated serine residue (bottom). bHLH, basic helix-loop-helix domain; ZIP, leucine zipper domain. **(H)** In vitro phosphorylation of WT and mutant His6-SMT3-TFE3(213–411) by CDK4/cyclin D1 complex and CDK6/cyclin D3 complex. Phosphorylated proteins were detected by autoradiography (upper panels), and the same gel was stained with Coomassie blue to visualize the total proteins (lower panels). Relative fold change of TFE3 phosphorylation in each mutant was normalized by total proteins. **(I)** Inhibition of TFE3 phosphorylation at Ser246 by LY2835219. HeLa cells expressing EGFP-TFE3 were treated with LY2835219 (1 µM, 2.5 µM, 3 h) and immunoprecipitated with GFP-Trap beads. The precipitated proteins were detected with antibodies against phospho-[TFEB(Ser142)/TFE3(Ser246)/MITF(Ser180)] (upper) and EGFP (lower). Relative fold change of phospho-TFE3(Ser246) was normalized by EGFP intensity. **(J)** Phosphorylation of Ser246 in TFE3 is decreased in CDK4 or CDK6 KO cells. Ctrl, CDK4 KO, and CDK6 KO cells were transfected with EGFP-TFE3 for 24 h and immunoprecipitated with GFP-Trap beads. The precipitated proteins were detected with antibodies against phospho-[TFEB(Ser142)/TFE3(Ser246)/MITF(Ser180)], EGFP, CDK4, and CDK6. Relative fold change of phospho-TFE3(Ser246) is normalized by EGFP intensity. **(K)** Images (left) and quantification (right) of the ratio of nucleus-localized WT EGFP-TFE3 and the EGFP-TFE3 mutants S246A, S568A, and S246A/S568A. Scale bars represent 10 µm in all images. For all quantifications, data (mean ± SEM) were from three independent experiments and were analyzed using one-way ANOVA with the post hoc Holm-Sidak test. ≥500 cells were quantified in each group. ***, P < 0.001. ns, not significant.

staining or FITC-Dextran labeling (Fig. 7 C). This suggests that TFEB and TFE3 are required for the lysosomal increase in the S–M phases. We then examined TFEB Ser142 phosphorylation in TFEB-EGFP–expressing HeLa cells sorted with flow cytometry and found that TFEB Ser142 phosphorylation was strongly reduced in the S–M phases compared with G1 (Fig. 7 D). In addition, in HeLa cells synchronized to individual cell cycle phases, the nuclear localization of TFEB and TFE3 markedly increased at the S–M phases compared with G1 (Fig. 7, E–G). Thus, the reduction of TFEB Ser142 phosphorylation and the increase in TFEB and TFE3 nuclear localization correlated well with the inactivation of CDK4 and CDK6 in the S–M phases. Taken together, these results provide further evidence that the CDK4/6–TFEB/TFE3 axis regulates lysosome biogenesis in the cell cycle (Fig. 7 H).

Inhibition of CDK4/6 promotes cellular clearance of various substrates

Finally, we examined if lysosomes induced by CDK4/6 inhibition are functional. LY2835219-induced lysosomes were positive for Magic Red, an indicator of active lysosomal protease cathepsin B (Fig. 8 A; Boonacker and Van Noorden, 2001; Van Noorden et al., 1997). This effect was inhibited by bafilomycin A1 (BFA1), an inhibitor of lysosomal acidification (Fig. 8 A). Similarly, LY2835219-induced LysoTracker Red–positive lysosomes were also positive for BODIPY–pepstatin A, which indicates the activation of the lysosomal protease cathepsin D (Fig. 8 B; Chen et al., 2000). Furthermore, LY2835219, like Torin 1, increased lysosomal protease activities measured with β-N-acetylglucosaminidase (NAG) assays (Fig. 8 C; Li et al., 2016). In HepG2 cells that were overloaded with oleic acid, LY2835219 treatment strongly reduced the number of lipid droplets, as did Torin 1 (Fig. 8 D). In the presence of the lysosomal inhibitor BFA1, neither LY2835219 nor Torin 1 reduced the number of lipid droplets (Fig. 8 D), indicating that they acted in a lysosome-dependent manner. In HeLa cells that express Htt97Q-GFP, LY2835219 and Torin 1 similarly reduced the accumulation of polyglutamine (polyQ) aggregates (Fig. 8 E). Altogether, these results suggest that inhibition of CDK4/6 promotes lysosomal activity and cellular clearance of a variety of substrates.

Discussion

It is not understood how intracellular organelles replicate themselves in order to be dispensed to daughter cells at mitotic cell division. Here, our findings define a mechanism that regulates lysosome biogenesis during the cell cycle. In cells with sufficient nutrients, pharmacological inhibition or genetic inactivation of CDK4/6 leads to nuclear retention and activation of TFEB and TFE3, consequently resulting in TFEB- and TFE3-dependent lysosome biogenesis and autophagy. Our results further revealed that CDK4 and CDK6 interact with and phosphorylate TFEB and TFE3 solely in the nucleus, because only nuclear TFEB and TFE3 coprecipitated with nuclear CDK4 and CDK6 as well as with their activators cyclin D1 and cyclin D3. CDK4/6 directly phosphorylate TFEB at Ser142 and TFE3 at Ser246 in the nucleus, as evidenced by the finding that LY2835219 failed to inhibit such phosphorylation when TFEB and TFE3 were prevented from translocating to the nucleus. A TFEB mutant that cannot be phosphorylated by CDK4/6 has a much weaker interaction with the CRM1 exportin than WT TFEB does, which suggests that CDK4/6–mediated phosphorylation is essential for CRM1-dependent nuclear export of TFEB/TFE3. In addition, it is possible that nuclear TFEB and TFE3, if not phosphorylated, have higher transcriptional activities. Thus, inhibition of CDK4/6 reduces the nucleo-cytoplasmic shuttling of TFEB and TFE3 and consequently enhances their activation.

Importantly, inhibitors of other major CDKs do not affect the subcellular localization of TFEB. These findings collectively
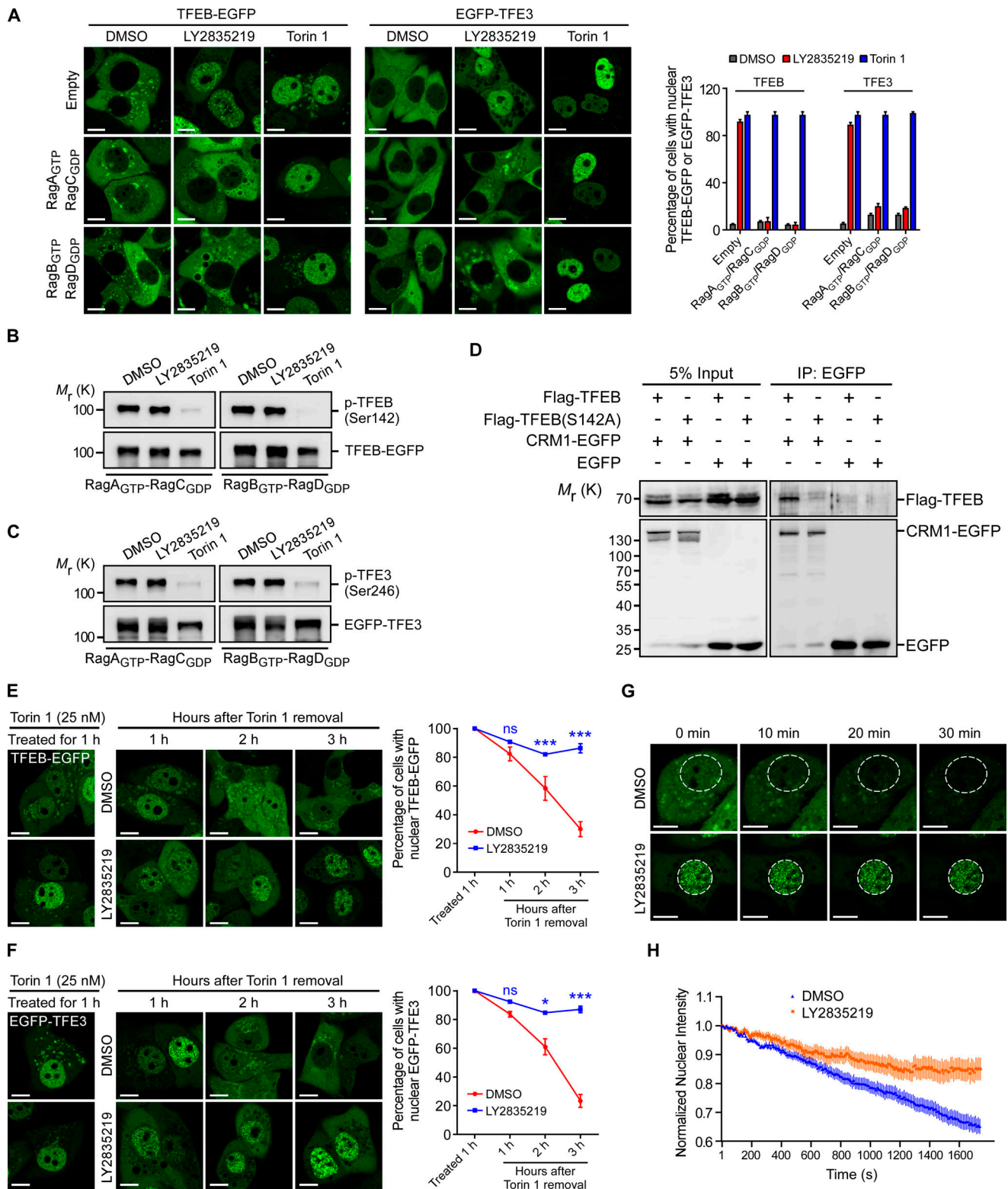
Figure 5. **Phosphorylation of TFEB and TFE3 by CDK4/6 is essential for their nuclear export. (A)** In HeLa cells expressing constitutively activated Rag complexes, inhibition of CDK4/6 prevents the nuclear localization of TFEB and TFE3. TFEB-EGFP or EGFP-TFE3 was coexpressed with $RagA_{GTP}$-$RagC_{GDP}$ or $RagB_{GTP}$-$RagD_{GDP}$. Cells were then treated with LY2835219 (1 µM, 3 h) and Torin 1 (1 µM, 3 h). Representative images (left and middle) and quantification (right) of nuclear TFEB-EGFP or EGFP-TFE3 are shown. ≥300 cells were quantified in each group. **(B and C)** LY2835219 does not inhibit TFEB p-Ser142 (B) or TFE3 p-Ser246 (C) in HeLa cells expressing activated Rag complexes. HeLa cells were treated as in A, and all samples were subjected to IP with GFP-Trap beads. Precipitated proteins were detected using antibodies against GFP and phospho-[TFEB(Ser142)/TFE3(Ser246)/MITF(Ser180)]. **(D)** Co-IP of Flag-TFEB or Flag-TFEB(S142A) with CRM1-EGFP. IPs were performed with GFP antibody, and precipitated proteins were detected with antibodies against Flag or GFP. **(E and F)** HeLa cells expressing TFEB-EGFP or EGFP-TFE3 were treated with Torin 1 (25 nM, 1 h) and then cultured in medium with either DMSO or LY2835219 (1 µM) for

the indicated times (1 h, 2 h, and 3 h). Representative images (left) and quantification (right) of nuclear TFEB-EGFP or EGFP-TFE3 at each time point are shown. ≥600 cells were quantified in each group. **(G)** Nuclear FLIP assays. HeLa cells expressing TFEB-EGFP were treated with Torin 1 (25 nM, 1 h) and then cultured in fresh medium without Torin 1 but containing DMSO or LY2835219 (1 µM) for 1 h 30 min. Cytosolic TFEB-EGFP was continuously photobleached for 30 min, and nuclear EGFP signals were analyzed. Representative images for the indicated time points in the FLIP experiment are shown. Nuclear regions indicated with white dashed circles were analyzed for decay of nuclear EGFP fluorescence. ≥17 cells were quantified for each treatment. **(H)** Normalized nuclear EGFP intensity in the FLIP assays in G. Scale bars represent 10 µm in all images. For all quantifications, data (mean ± SEM) were from three independent experiments and were analyzed using one-way ANOVA with the post hoc Holm-Sidak test. *, P < 0.05; ***, P < 0.001. ns, not significant.

suggest that CDK4 and CDK6, rather than other CDKs, regulate lysosome biogenesis through TFEB and TFE3 in the cell cycle. Supporting this conclusion, Ser142 phosphorylation of TFEB is markedly reduced and nuclear retention of TFEB and lysosome biogenesis are greatly increased in the S–M phases, concomitant with the decline of cyclin D1, the essential activator of CDK4/6. Thus, the high activities of CDK4/6 suppress lysosome biogenesis at the G1 phase, while their low activities enhance lysosome biogenesis in the S–M phases by relieving the inhibition of TFEB and TFE3 (Fig. 7 H).

Phosphorylation of cytoplasmic TFEB and TFE3 keeps them in the cytoplasm, where they are inactive. On the lysosome, mTOR phosphorylates TFEB (Ser211 and Ser142) and TFE3 (Ser321 and Ser246), leading to their lysosomal release and subsequent interaction with 14-3-3 proteins in the cytoplasm (Martina et al., 2012, 2014; Roczniak-Ferguson et al., 2012; Settembre et al., 2012; Vega-Rubin-de-Celis et al., 2017). TFEB Ser142, and probably TFE3 Ser246, can also be phosphorylated by ERK (Settembre et al., 2011, 2012). Under some circumstances, TFEB might be phosphorylated at Ser3 by MAP4K3 or at Ser122 by mTOR (Hsu et al., 2018; Vega-Rubin-de-Celis et al., 2017). When cells are devoid of nutrients, mTOR is inactivated and fails to phosphorylate TFEB and TFE3. In the meantime, lysosomal calcium efflux is induced, which activates calcineurin to dephosphorylate existing phosphorylated TFEB and TFE3 (Medina et al., 2015; Wang et al., 2015). This leads to their nuclear translocation and activation. In addition to nutrient signaling, GSK3β phosphorylates TFEB (Ser134 and Ser138) to promote its lysosomal localization (Li et al., 2016). It remains to be determined whether phosphorylation of TFEB at Ser142 by mTOR or ERK primes GSK3β-dependent Ser138 and Ser134 phosphorylation. However, activation of PKC leads to GSK3β phosphorylation and inactivation without compromising mTOR, resulting in TFEB dephosphorylation and nuclear translocation (Li et al., 2016). Thus, cytoplasmic phosphorylation by mTOR, ERK, GSK3β, and other kinases maintains TFEB and TFE3 in a cytoplasmic and inactive state (Puertollano et al., 2018). Interestingly, recent studies suggest that mTOR and probably GSK3β also phosphorylate TFEB (Ser142 and Ser138) in the nucleus, promoting its CRM1-mediated nuclear export and inactivation (Li et al., 2018; Napolitano et al., 2018). Nevertheless, further investigation is required to determine whether mTOR and GSK3β indeed localize and function in the nucleus (Napolitano et al., 2018).

Our findings clearly demonstrated that in cells with sufficient nutrients, CDK4/6 are the kinases that phosphorylate TFEB and TFE3 in the nucleus, especially at the G1 phase of the cell cycle. It is likely that after being exported into the cytoplasm, Ser142-phosporylated TFEB is further phosphorylated at Ser138 and

Ser134 by GSK3β, promoting its cytoplasmic localization. Alternatively, CDK4/6 phosphorylation of TFEB at Ser142 may prime the phosphorylation at Ser138 and Ser134 by GSK3β in the nucleus at the G1 phase, if GSK3β indeed has a nuclear role. In the S–M phases, cyclin D1 is exported through the CRM1 exportin to the cytoplasm and subsequently degraded by the 26S proteasome (Alt et al., 2000; Diehl et al., 1998, 1997). This switches off CDK4/6 activity and consequently TFEB Ser142 phosphorylation, thus activating TFEB and TFE3 by retaining them in the nucleus.

CDK4/6 inhibitors including LY2835219 and PD0332991 are currently being used or are under clinical trial for cancer therapy (Asghar et al., 2015; Goel et al., 2018; Lim and Kaldis, 2013; Qie and Diehl, 2016; Sherr et al., 2016). Our findings that CDK4/6 inhibitors induce lysosome biogenesis and autophagy have implications for the use of CDK4/6 inhibitors in cancer treatment, because autophagy has differential impacts on distinct phases in tumorigenesis (Acevedo et al., 2016; Galluzzi et al., 2015; Valenzuela et al., 2017; Vijayaraghavan et al., 2017). Moreover, it will be valuable to evaluate the potential use of CDK4/6 inhibitors for treatment of lysosome-related disorders based on our findings that CDK4/6 inhibitors promote lysosome functions and cellular clearance.

Materials and methods

Cell culture, transfection, and reagents

All cell lines used in this work were obtained from ATCC. Cells were cultured at 37°C with 5% CO_2 in DMEM (Gibco) with 10% heat-inactivated FBS (BioInd), 100 U/ml penicillin, and 100 µg/ml streptomycin. Cells were tested for mycoplasma contamination using DAPI staining, and all test results were negative. Transient transfections were performed with Lipofectamine 2000 (Invitrogen) according to the manufacturer's instructions. Other reagents involved in this study are listed in Table S2.

Generation of CDK4 and CDK6 KO HeLa cells

CDK4 and CDK6 KO cells were generated using CRISPR/Cas9 technology. The CDK4 guide RNA, CDK4sgRNA1 (5′-CACCGA TCTCGGTGAACGATGCAAT-3′), was cloned into the pSpCas9 (BB)–2A-GFP (PX458) vector (Addgene; plasmid 48138) and transfected into HeLa cells. 72 h later, GFP-positive cells were sorted by FACS and cultured for 10 d. 48 colonies were picked and examined for deletion in the CDK4 gene by PCR and Western blotting. CDK4 deletion was further confirmed by sequencing. Similar strategies were applied to generate CDK6-KO cells using the CDK6 guide RNA, CDK6sgRNA1 (5′-CACCGTTAG ATCGCGATGCACTACT-3′).
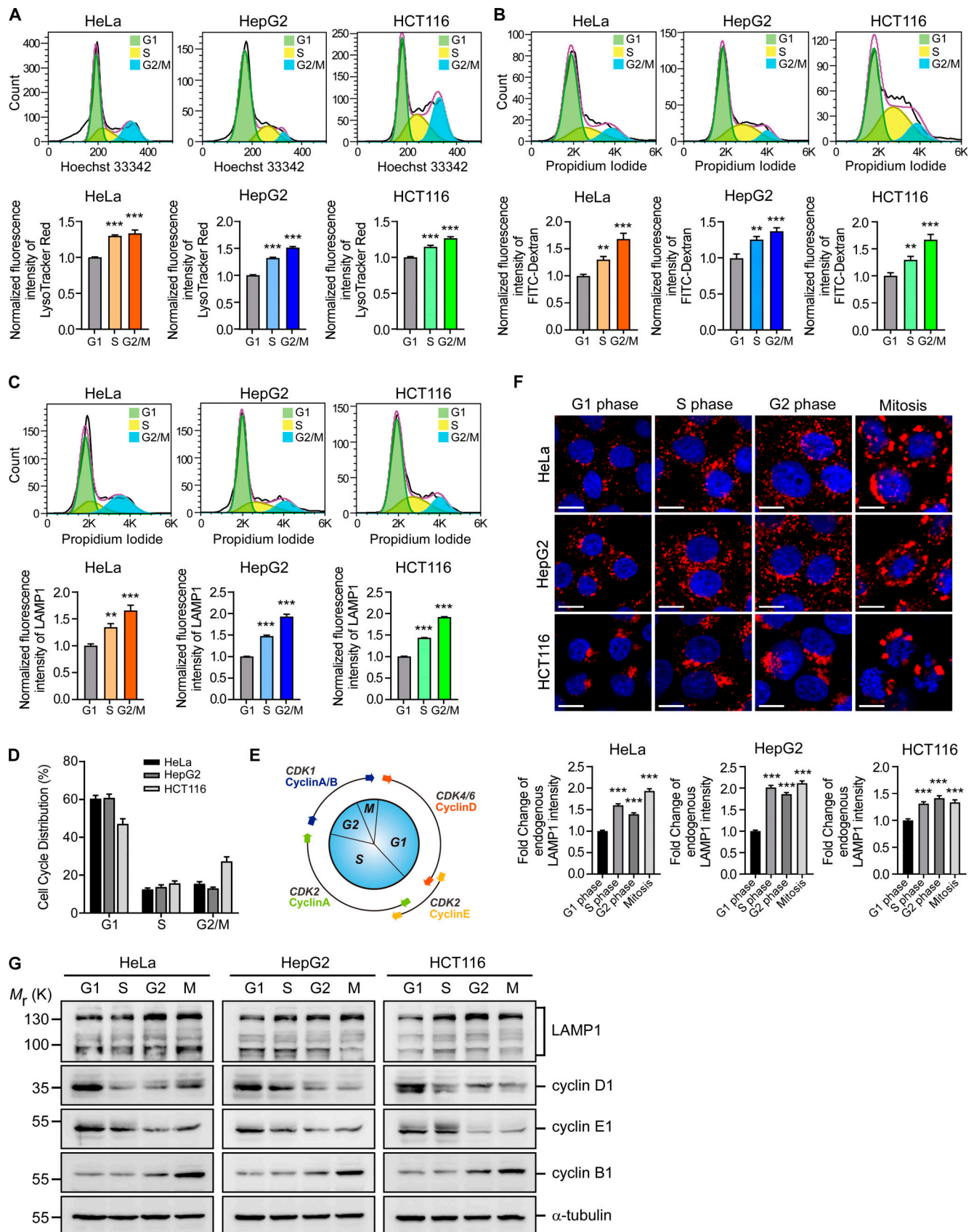
Figure 6. Cell cycle–dependent lysosome biogenesis. (A) HeLa, HepG2, and HCT116 cells were stained with LysoTracker Red and Hoechst 33342 for 30 min. Cells were sorted by FACS to determine their phases in the cell cycle. Upper row: Representative cell cycle histograms of the indicated cell types. Lower row:

Quantification of LysoTracker Red intensity to determine the relative abundance of lysosomes in each phase of the cell cycle. **(B)** HeLa, HepG2, and HCT116 cells were incubated with FITC-Dextran for 12 h and stained with PI. Cells were sorted by FACS to determine their phases in the cell cycle. Upper row: representative cell cycle histograms of the indicated cells. Lower row: quantification of FITC-Dextran intensity to determine the relative abundance of lysosomes in each phase of the cell cycle. **(C)** HeLa, HepG2, and HCT116 cells were immunostained with LAMP1 antibody and PI. Cells were sorted by FACS to determine their phases in the cell cycle. Upper row: representative cell cycle histograms of the indicated cell types. Lower row: quantification of LAMP1 immunostaining intensity to determine the relative abundance of lysosomes in each cell cycle phase. **(A–C)** Data (mean ± SEM) were from three independent experiments, and comparisons are made between G1 and other phases of the cell cycle. Cell cycle histograms were analyzed by PI or Hoechst 33342 content and fitted to the Dean-Jett-Fox cell cycle model using FlowJo software. The purple lines in the histograms represent the curve-fitting of cell cycle phases by FlowJo, and the black lines represent the curve generated by the samples. **(D)** Quantitative analysis of the distribution of cell cycle phases in HeLa, HepG2, and HCT116 cells. **(E)** Schematic description of the activity of CDKs/cyclins in the cell cycle. **(F)** HeLa, HepG2, and HCT116 cells were synchronized to G1, S, G2, and M phases using standard assays. Representative images (upper) and quantification (lower) of endogenous LAMP1 immunostaining are shown for the indicated cell types. ≥80 cells were quantified for each cell cycle phase. **(G)** Immunoblotting of LAMP1, cyclin D1, cyclin E1, cyclin B1, and α-tubulin in HeLa, HepG2, and HCT116 cells synchronized to G1, S, G2, and M phases. Scale bars represent 10 μm in all images. For all quantifications, data (mean ± SEM) were from three independent experiments and were analyzed using one-way ANOVA with the post hoc Holm-Sidak test. **, $P < 0.01$; ***, $P < 0.001$.

siRNA
RNA oligonucleotides used for siRNA are listed in Table S3. Cells grown in 6-well plates or confocal dishes were transfected with 100 pmol RNA oligonucleotides using Lipofectamine 2000 according to the manufacturer's instructions. Cells were harvested for further experiments 48 h after transfection. The efficiency of siRNAs was evaluated by Western blotting.

Antibodies
The antibodies used in this study are listed in Table S4.

Examination of lysosomes and lysosomal activities
Cells grown on glass-bottom dishes (Cellvis) were treated with individual compounds for 3 h and further cultured in fresh medium containing LysoTracker Red DND-99 (0.3 μM) for 30 min. Cells were then changed to LysoTracker-free medium and observed by confocal microscopy. To assess cathepsin B and cathepsin D activities, cells were treated with individual compounds for 3 h, followed by staining with Magic Red substrates (ImmunoChemistry Technologies) or BODIPY FL–pepstatin A (1 μM) according to the manufacturer's instruction.

NAG assays were performed using a kit from Sigma-Aldrich (CS0780). HeLa cells were treated with different concentrations of LY2835219 or Torin 1 (1 μM) for 3 h and lysed with RIPA buffer. Total protein concentration was determined with the BCA Protein Assay Kit (Thermo Fisher Scientific). NAG activity was measured in 20 μg cell lysate from each sample.

Immunostaining and confocal microscopy
For immunostaining, cells grown on glass-bottom dishes or coverslips were fixed with 4% PFA in PBS at room temperature for 15 min and permeabilized with 0.5% saponin (Sigma-Aldrich) in PBS at room temperature for another 15 min. Cells were incubated with primary antibodies in the staining buffer (1% BSA and 0.05% saponin in PBS) at 4°C overnight. In colocalization experiments, cells were permeabilized with 0.1% Triton X-100 for 5 min and then incubated with blocking buffer (1% BSA, 0.3 M glycine, and 0.1% Tween 20 in PBS) for 1 h. Cells were then incubated with primary antibodies in the staining buffer (1% BSA and 0.1% Tween 20 in PBS) at 4°C overnight. Dilution of individual antibodies is listed in Table S4. Cells were washed three times in PBS and incubated with Alexa Fluor 488– or Alexa Fluor 568–conjugated secondary antibodies for 1 h at room temperature. Cells were washed three times, then stained with DAPI (Sigma-Aldrich). All samples were visualized using a Zeiss LSM 880 inverted Confocal Laser Scanning Microscope with Airyscan and an inverted Olympus FV1000 confocal microscope. Images in colocalization experiments were obtained with Airyscan super-resolution mode using an α Plan-Apochromat 100×/1.46 oil immersion objective lens and were processed and analyzed with ZEN 2 (blue edition), FV10-ASW 4.0a Viewer, or ImageJ (National Institutes of Health).

FLIP assays
HeLa cells expressing TFEB-EGFP were grown on 35-mm glass-bottom dishes and treated with 25 nM Torin 1 for 1 h, which was replaced with fresh DMEM medium containing either DMSO or LY2835219 (1 μM) for 1.5 h. The FLIP assays were then performed on a Zeiss LSM 880 Confocal Microscope using a 63× oil immersion objective lens with a 488-nm laser excitation. The cytosol of cells was designated as the photobleaching region, and the fluorescence intensities of the nucleus were acquired for analysis. After scanning for five frames, the cytosol was bleached with three iterations at 5% power, and the nuclear fluorescence was monitored every 10 s at 2–3% power within 30 min. A fluorescent region from an adjoining cell in the same field was used to correct for general photobleaching. The data were generated by fitting in a double exponential decay model using Zen software (Zeiss). Nuclear fluorescence intensity values at each time point were normalized with the start time point. Quantification of normalized nuclear intensity was generated by GraphPad Prism (8.0.1).

Western blotting and IPs
For Western blotting, cells were lysed in ice-cold RIPA buffer (20 mM Tris-HCl, pH 7.5, 100 mM NaCl, 0.1% SDS, 0.5% sodium deoxycholate, and 1 mM PMSF) containing Complete Protease Inhibitor Cocktail and Phosphatase Inhibitor Cocktail (Roche). Cell lysates were centrifuged at 13,000 rpm for 15 min, and 20 μg of total proteins was resolved by SDS-PAGE and probed with the indicated antibodies (Table S4). The amount of α-tubulin was used as the loading control. Blots were developed with chemiluminescent detection reagent (ECL; GE Healthcare and Thermo Fisher Scientific) and imaged with a Smartchemi machine (Sage Creation). Quantification of Western blots was performed using ImageJ software.
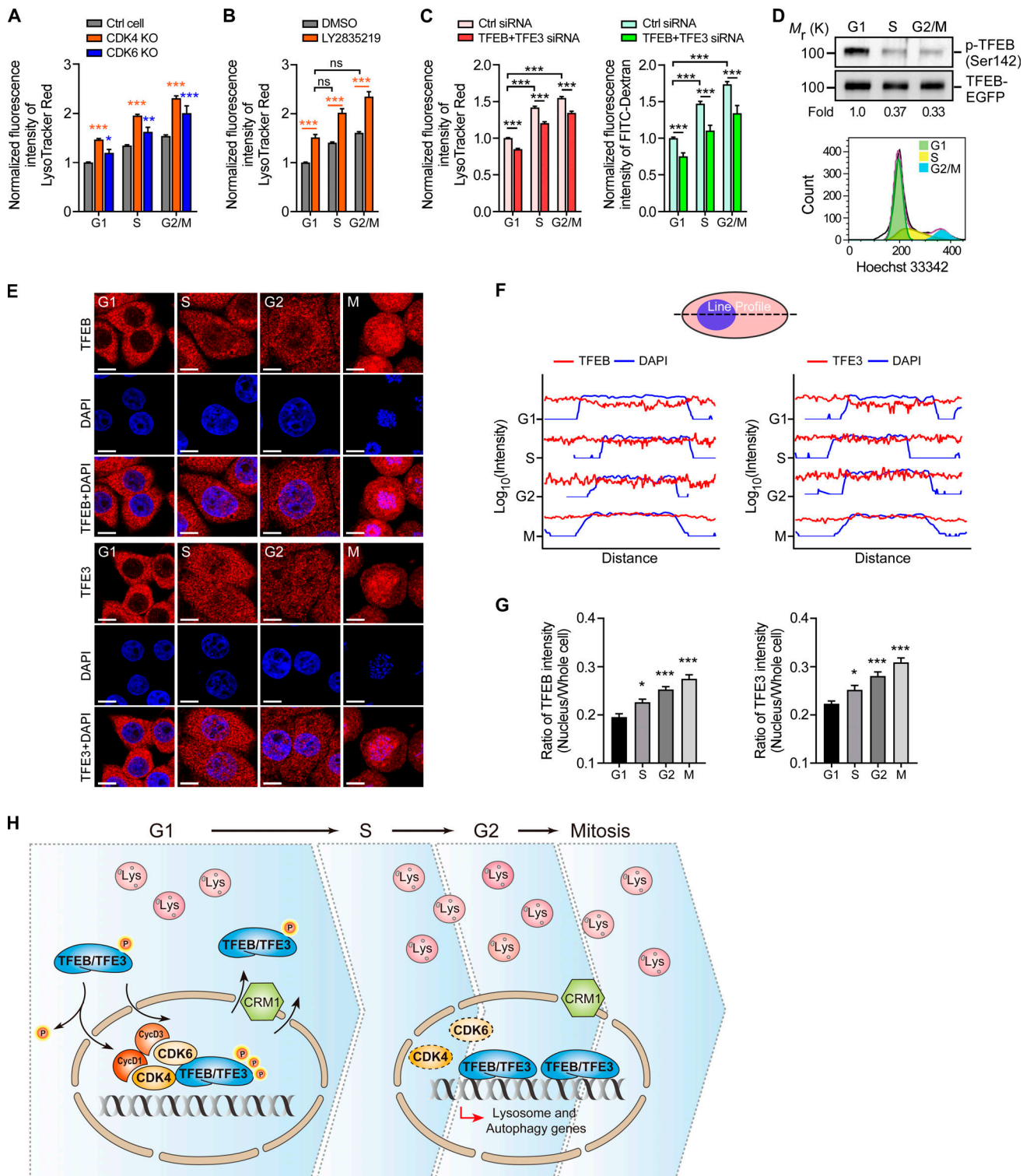
Yin et al.
Lysosome biogenesis in the cell cycle

Journal of Cell Biology   14 of 20
https://doi.org/10.1083/jcb.201911036

Figure 7. **CDK4/6 regulate cell cycle–dependent lysosome biogenesis. (A)** Control (Ctrl), CDK4 KO, and CDK6 KO cells were stained with LysoTracker Red and Hoechst 33342 for 30 min. Cells were analyzed by FACS to determine their phases in the cell cycle. The bar chart shows quantification of LysoTracker Red intensity to determine the relative abundance of lysosomes in each phase of the cell cycle in Ctrl, CDK4 KO, and CDK6 KO cells. Comparisons are made between Ctrl and KO cells in each phase. **(B)** HeLa cells were treated with DMSO or LY2835219 (0.5 µM, 12 h) and stained with LysoTracker Red and Hoechst 33342 for 30 min. Cells were analyzed by FACS to determine their phases in the cell cycle. The bar chart shows quantification of LysoTracker Red intensity of cells in each phase. **(C)** HeLa cells were treated with Ctrl siRNA or TFEB+TFE3 siRNA for 48 h and stained with LysoTracker Red and Hoechst 33342 or FITC-Dextran and PI. Cells were analyzed by FACS to determine their phases in the cell cycle. The bar charts show quantification of LysoTracker Red intensity (left) and FITC-Dextran intensity (right) to determine the relative abundance of lysosomes in each phase of the cell cycle. **(D)** Phosphorylation of Ser142 in TFEB is decreased in the S and G2/M phases. HeLa cells expressing TFEB-EGFP were stained with Hoechst 33342 for 30 min and sorted by FACS based on the DNA content of G1, S, and G2/M phases. Enriched cells were immunoprecipitated with GFP-Trap beads and detected with antibodies against phospho-[TFEB(Ser142)/

TFE3(Ser246)/MITF(Ser180)] and EGFP (upper). Relative fold change of phospho-TFEB (Ser142) is normalized by EGFP intensity. Histogram of sorted cells (lower) analyzed by Hoechst 33342 content and fitted to the Dean-Jett-Fox cell cycle model using FlowJo software. **(E)** Representative images showing TFEB and TFE3 subcellular localization in cells synchronized to individual cell cycle phases. Endogenous TFEB and TFE3 were stained with individual antibodies. **(F)** Fluorescence intensities (red line) of TFEB (left), TFE3 (right), and DAPI (blue line) in representative cells in E were measured along a line across the cytosol and nucleus (top diagram). Data were $\log_{10}$ transformed to show the fluctuation of fluorescence intensity. **(G)** Quantification of the ratio of nucleus/whole cell fluorescence intensity of TFEB (left) and TFE3 (right) in cells as shown in E. ≥50 cells were quantified for each cell cycle phase. **(H)** Graphic summary of cell cycle–dependent lysosome biogenesis. At the G1 phase, CDK4/6 are activated by D-type cyclins. The activated kinases then interact with and phosphorylate TFEB and TFE3, promoting their nuclear export and inactivation. During S to M phases, CDK4/6 are inactivated owing to cyclin D turnover. TFEB and TFE3 are not phosphorylated by CDK4/6 and thus are retained in the nucleus, where they promote lysosome biogenesis and autophagy. Lys, lysosome. Scale bars represent 10 µm in all images. For all quantifications, data (mean ± SEM) were from three independent experiments and were analyzed using one-way ANOVA with the post hoc Holm-Sidak test. *, $P < 0.05$; **, $P < 0.01$; ***, $P < 0.001$. ns, not significant.

For IPs of GFP- or FLAG-tagged proteins, cells were lysed in IP buffer (50 mM Tris-HCl, pH 7.5, 150 mM NaCl, 1% NP-40, 1 mM PMSF, and 1% glycerol) containing Complete Protease Inhibitor Cocktail and Phosphatase Inhibitor Cocktail. Cell lysates were centrifuged at 13,000 rpm for 15 min at 4°C, and the clear supernatants were incubated with either FLAG antibody (M2)–conjugated beads (Sigma-Aldrich) or GFP beads (ChromoTek) overnight at 4°C. The beads were centrifuged and extensively washed in wash buffer. Precipitated proteins were resolved by SDS-PAGE, then blotted and detected with different antibodies.

Co-IPs of endogenous CDK4, CDK6, cyclin D1, or cyclin D3 with TFEB or TFE3 were performed with cytosolic and nuclear fractions. For fractionation, cells were first lysed in cytosol lysis buffer (10 mM Hepes, pH 7.8, 15 mM KCl, 1 mM MgCl$_2$, 0.1 mM EDTA, 1 mM DTT, 1 mM PMSF, and 10% glycerol) containing Complete Protease Inhibitor Cocktail and Phosphatase Inhibitor Cocktail and ground with a tissue homogenizer. Lysates were centrifuged at 1,100× g for 10 min at 4°C. The supernatant was collected and adjusted to 100 mM NaCl and 0.1% NP-40 and used as the cytosolic fraction for IP. The pellets were washed once with the cytosol lysis buffer and lysed in the nucleus lysis buffer (50 mM Hepes, pH 7.8, 3 mM MgCl$_2$, 300 mM NaCl, 1 mM DTT, 0.1 mM PMSF, 10% NP-40, and 10% glycerol) containing Benzonase Nuclease (Sigma-Aldrich) for 1 h at 4°C. The nuclear lysate was adjusted to 100 mM NaCl and 0.1% NP-40 and cleared by centrifugation at 10,000× g for 10 min. The cleared nuclear lysate was further used for IP. The cytosolic and nuclear protein lysates were incubated with primary antibodies of CDK4, CDK6, cyclin D1, and cyclin D3 overnight at 4°C and further incubated with Protein A agarose beads (Thermo Fisher Scientific) for an additional 4 h at 4°C. After extensive washing, precipitated proteins were resolved by SDS-PAGE, then blotted and probed with different antibodies.

In vitro kinase assays
Active GST-CDK4/cyclin D1 complex (Product Number 0142–0143-1) and GST-CDK6/cyclin D3 complex (Product Number 0051–0373-1) used in this study were purchased from ProQinase GmbH. Purified His6-SMT3-TFEB or His6-SMT3-TFE3 proteins (2 µg) immobilized on Ni-chelating Sepharose beads were incubated with CDK4/cyclin D1 complex or CDK6/cyclin D3 complex (1 µg of each) for 2 h at 30°C in 30 µl kinase buffer (25 mM Hepes, pH 7.4, 50 mM NaCl, 5 mM MgCl$_2$, 1 mM CaCl$_2$, 1 mM DTT, and 30 µM ATP) containing 1.0 µCi of [γ-^{32}P]ATP (Perkin Elmer).

After extensive washing, proteins bound on beads were resolved by SDS-PAGE, and phosphorylation signals were detected using autoradiography. The same gels were subsequently stained with Coomassie blue to visualize the total proteins.

Mass spectrometry
For mass spectrometry analysis, phosphorylation reactions were performed without adding [γ-^{32}P] ATP and resolved on SDS-PAGE. His6-SMT3-TFEB protein bands were excised and subjected to an in-gel trypsin digest. The tryptic peptides were then analyzed by liquid chromatography–tandem mass spectrometry using an LTQ Orbitrap Elite mass spectrometer (Thermo Fisher Scientific) coupled online to an Easy-nLC 1000 in the data-dependent mode. Data were analyzed by Thermo Scientific Proteome Discoverer software version 1.4 to compare the phosphorylation of TFEB proteins.

Plasmids and site-directed mutagenesis
The mammalian and bacterial expression vectors were constructed using standard protocols, and details of plasmids are listed in Table S5. All constructs were confirmed by sequencing. Mutations were generated by PCR-mediated mutagenesis using the oligonucleotide pairs listed in Table S6.

Detection of the TFEB phospho-142 or TFE3 phospho-246
Cells expressing TFEB-EGFP and EGFP-TFE3 were lysed in lysis buffer (25 mM Tris-HCl, pH 7.5, 150 mM NaCl, 0.5 mM EDTA, and 0.1% NP-40) containing Complete Protease Inhibitor Cocktail and Phosphatase Inhibitor Cocktail for 1 h on ice. Lysates were centrifuged at 13,000 rpm for 15 min, and then the lysates were incubated with 10 µl of GFP-Trap agarose beads (Chromotek) for 2 h at 4°C. After extensive washing, proteins were precipitated and resolved by SDS-PAGE, blotted, and probed with GFP antibody and an antibody that recognizes p-Ser142 of TFEB, p-Ser246 of TFE3, and p-Ser180 of MITF (phospho–[TFEB(Ser142)/TFE3(Ser246)/MITF(Ser180)]). This antibody was generated by using a synthetic Ser180 phosphopeptide derived from human MITF, which is conserved with Ser142 in TFEB and Ser246 in TFE3 (PA5-36755; Invitrogen).

Analysis of lysosomes during the cell cycle
HeLa, HepG2, and HCT116 cells were costained with LysoTracker Red (0.3 µM) and Hoechst 33342 for 30 min. After extensive washing, cells were suspended in cold PBS and analyzed by flow
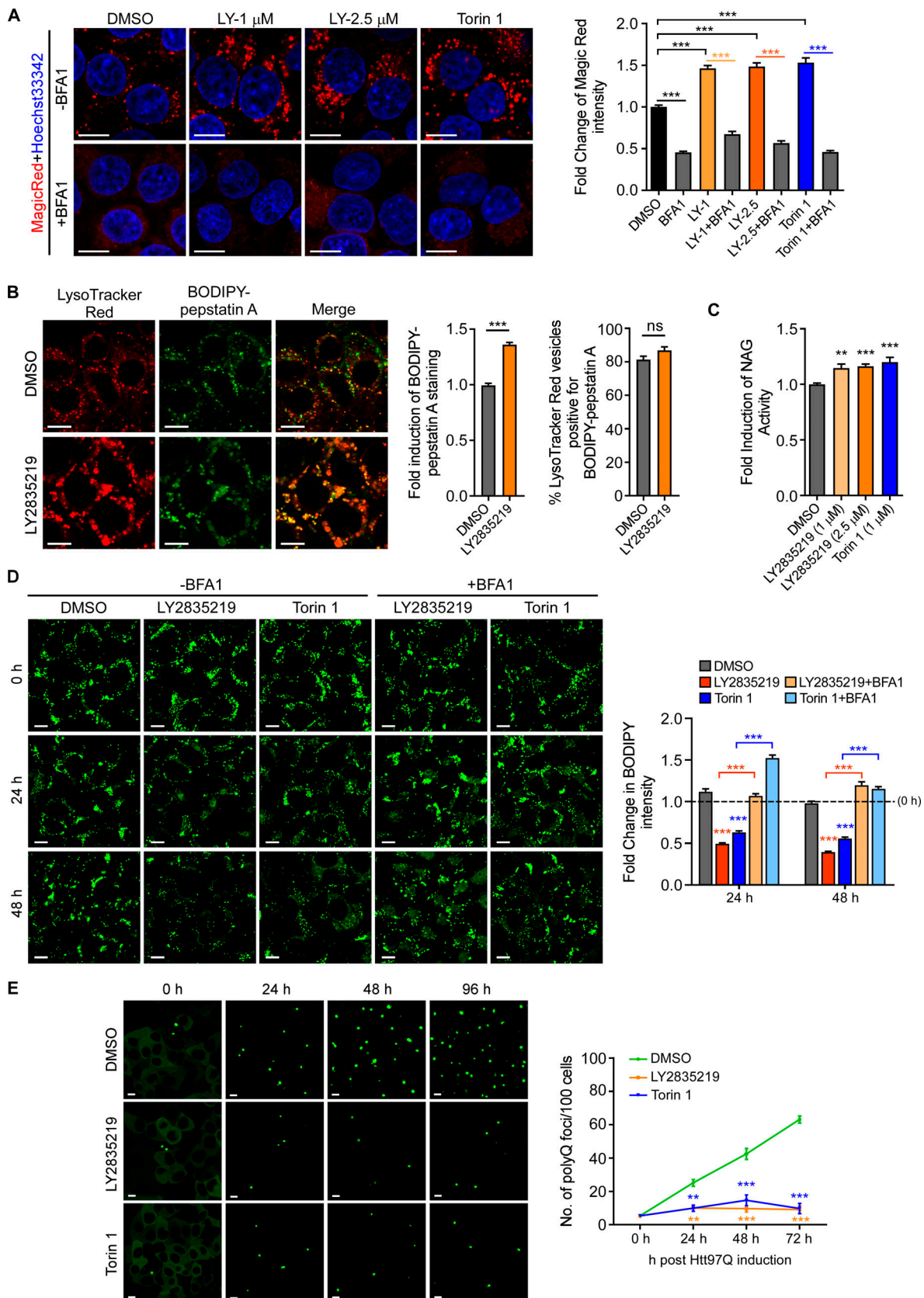
Figure 8. **Inhibition of CDK4/6 promotes cellular clearance. (A)** LY2835219 enhances Magic Red staining. HeLa cells were treated with LY2835219 (1 μM, 2.5 μM, 3 h) or Torin 1 (1 μM, 3 h) with or without BFA1 (0.4 μM, 3 h) and stained with Magic Red. Left: Representative images of Magic Red staining. Nuclei are stained with Hoechst 33342. Right: Quantifications (fold change) of Magic Red intensity. LY, LY2835219. ≥30 cells were quantified for each treatment. **(B)**

Images (left) and quantifications (right) of HeLa cells treated with LY2835219 (1 µM, 3 h) and costained with BODIPY–pepstatin A (1 µM) and LysoTracker Red. ≥180 cells were quantified for fold induction of BODIPY–pepstatin A. ≥30 cells were quantified for the percentage of vesicles positive for LysoTracker Red and BODIPY–pepstatin A. **(C)** Relative lysosomal NAG activity of LY2835219- and Torin 1–treated HeLa cells. **(D)** HepG2 cells were fed with oleic acid (100 µM, 12 h) to induce lipid droplet formation. Cells were treated with LY2835219 (0.5 µM) or Torin 1 (0.5 µM) with or without BFA1 (0.1 µM) at the indicated times after withdrawal of oleic acid. Lipid droplets were stained with BODIPY (left). Quantification (right) of BODIPY intensity at each time point was normalized to the start point. The dashed line indicates the BODIPY intensity at the start (0 h). ≥100 cells were quantified for each treatment. **(E)** HeLa cells stably expressing Tet-on Htt97Q-GFP were treated with doxycycline (1 µg/ml) for 12 h. After removal of doxycycline, cells were treated with LY2835219 (0.5 µM) or Torin 1 (0.5 µM) for the indicated times. The number of polyQ foci was quantified at the indicated time points. Images (left) and quantification (right) of polyQ foci are shown. ≥300 cells were quantified for each treatment. Scale bars represent 10 µm in all images. For all quantifications, data (mean ± SEM) were from three independent experiments and were analyzed using the unpaired two-tailed *t* test or one-way ANOVA with the post hoc Holm-Sidak test. **, $P < 0.01$; ***, $P < 0.001$. ns, not significant.

cytometry. For LAMP1 immunostaining, cells were first fixed with 4% PFA for 15 min and permeabilized with permeabilization buffer (1× PBS, 0.3% Triton X-100, and 0.5% BSA) for 15 min and incubated with LAMP1 antibody in the incubation buffer (0.5% BSA in PBS) for 1.5 h at room temperature. After extensive washing, cells were resuspended in incubation buffer containing Alexa Fluor 488 secondary antibody for 30 min. Cells were then collected and incubated in PI/RNase staining buffer (4087; Cell Signaling Technology) for an additional 30 min and analyzed by flow cytometry. For the FITC-Dextran experiment, cells were fed with 0.25 mg/ml FITC-Dextran for 12 h followed by 2-h recovery in fresh DMEM medium. Cells were then fixed with 70% ethanol (2 h, 4°C) and stained with PI for 30 min and analyzed by flow cytometry. All samples were analyzed on a FACSAria SORP machine (BD Biosciences), and the fluorescence intensity profiles of each cell cycle stage were analyzed using BD FACSDiva 8.0.1. Cell cycle distribution was analyzed by PI or Hoechst 33342 content and fitted to the Dean-Jett-Fox cell cycle model using FlowJo software.

Synchronization of cells
Synchronization of HeLa, HepG2, and HCT116 cells was performed as described (Ma and Poon, 2011). Briefly, cells were cultured in 100-mm dishes to 40–50% confluency. G1-phase synchronization was performed by lovastatin (20 µM) treatment for 24 h. A double thymidine block procedure was used to synchronize cells in S phase. Cells were first incubated with thymidine (2 mM) for 14 h (first thymidine block). After extensive washing, cells were then incubated with deoxycytidine (24 µM) for 9 h. Thymidine (2 mM) was added again, and the incubation was continued for another 14 h (second thymidine block). Cells were extensively washed again with PBS, then supplemented with deoxycytidine (24 µM) and incubated at 37°C. S-phase cells were immediately collected and analyzed. G2-phase cells were synchronized by treatment with the CDK inhibitor RO3306. After release from the second thymidine block, cells were allowed to recover for 2 h and then incubated with RO3306 (10 µM) for 10 h. M-phase cells were enriched by treating with nocodazole and mechanical shake-off. After release from the second thymidine block, cells were first grown for 2 h, and then incubated with nocodazole (0.1 µg/ml) for 10 h. M-phase cells, which were rounded and less attached to the dishes, were collected by mechanical shake-off. Cells synchronized at different stages were harvested and immunostained with LAMP1 antibody. Western blotting was performed to examine the levels of LAMP1, cyclin D1, cyclin E, and cyclin B. The reagents used in cell synchronization are listed in Table S2.

Quantitative RT-PCR (qRT-PCR)
Total RNA was extracted from cells using TRIzol Reagent (Invitrogen) and chloroform. 2 µg RNA was used as a template to generate cDNAs using the GoScript Reverse Transcription System (Promega). qRT-PCR reactions were performed on a CFX96 Real Time System C1000 Touch Thermal Cycler (BioRad). *GAPDH* was used as the endogenous reference gene. The primers for TFEB-targeted genes are listed in Table S7.

Lipid droplet clearance assay
HepG2 cells seeded in 35-mm glass-bottom dishes (Cellvis) were fed with oleic acid (100 µM, 12 h) to induce lipid droplet formation. After brief washing, cells were cultured in fresh DMEM medium containing LY2835219 (0.5 µM) or Torin 1 (0.5 µM) without or with BFA1 (0.1 µM) to different time points. Cells were stained with BODIPY (1 µg/ml) for 30 min at 37°C before examination with confocal microscopy.

Htt polyQ clearance assay
HeLa cells stably expressing Tet-on Htt97Q–GFP were incubated with doxycycline (1 µg/ml, 12 h) to induce Htt97Q-GFP expression (Li et al., 2016). Cells were briefly washed to remove doxycycline and further cultured in DMEM medium containing LY2835219 (0.5 µM) or Torin 1 (0.5 µM) to different time points. PolyQ foci were observed under a confocal microscope.

Statistical analysis
Data were analyzed with GraphPad Prism Software (8.0.1) to generate curves and bar charts. Statistically significant differences between two groups were determined by using the unpaired two-tailed *t* test. Statistically significant differences in experiments with more than two conditions were determined by one-way ANOVA with the post hoc Holm-Sidak test. *, $P < 0.05$; **, $P < 0.01$; ***, $P < 0.001$; $P > 0.05$ was considered not significant.

Online supplemental material
Fig. S1 shows that CDK4/6 inhibitors induce lysosome biogenesis. Fig. S2 illustrates that the inactivation of CDK4/6 has no direct effect on mTOR, ERK2, AKT, GSK3β, and PKC activities. Fig. S3 shows that cyclin D1 and cyclin D3 interact with TFEB and TFE3. Fig. S4 shows the results of mass spectrometry analysis of

the phosphorylated sites in TFEB(105–300) after treatment with CDK4/cyclin D1 or CDK6/cyclin D3 complex. Fig. S5 shows that CDK4 and CDK6 are essential for TFEB and TFE3 nuclear export. Table S1 shows the effects of other CDK inhibitors on TFEB translocation. Table S2 lists chemical compounds and reagents used in the study. Table S3 lists siRNA oligos used in the study. Table S4 lists all antibodies used in the study. Table S5 summarizes the expression vectors used in this study. Table S6 lists the oligos for site-directed mutagenesis. Table S7 lists the primers for qRT-PCR.

Acknowledgments

References

Acevedo, M., M. Vernier, L. Mignacca, F. Lessard, G. Huot, O. Moiseeva, V. Bourdeau, and G. Ferbeyre. 2016. A CDK4/6-Dependent Epigenetic Mechanism Protects Cancer Cells from PML-induced Senescence. Cancer Res. 76:3252–3264. https://doi.org/10.1158/0008-5472.CAN-15-2347

Alao, J.P.. 2007. The regulation of cyclin D1 degradation: roles in cancer development and the potential for therapeutic invention. Mol. Cancer. 6:24. https://doi.org/10.1186/1476-4598-6-24

Alt, J.R., J.L. Cleveland, M. Hannink, and J.A. Diehl. 2000. Phosphorylation-dependent regulation of cyclin D1 nuclear export and cyclin D1-dependent cellular transformation. Genes Dev. 14:3102–3114. https://doi.org/10.1101/gad.854900

Asghar, U., A.K. Witkiewicz, N.C. Turner, and E.S. Knudsen. 2015. The history and future of targeting cyclin-dependent kinases in cancer therapy. Nat. Rev. Drug Discov. 14:130–146. https://doi.org/10.1038/nrd4504

Baldin, V., J. Lukas, M.J. Marcote, M. Pagano, and G. Draetta. 1993. Cyclin D1 is a nuclear protein required for cell cycle progression in G1. Genes Dev. 7:812–821. https://doi.org/10.1101/gad.7.5.812

Boonacker, E., and C.J. Van Noorden. 2001. Enzyme cytochemical techniques for metabolic mapping in living cells, with special reference to proteolysis. J. Histochem. Cytochem. 49:1473–1486. https://doi.org/10.1177/002215540104901201

Chen, C.S., W.N. Chen, M. Zhou, S. Arttamangkul, and R.P. Haugland. 2000. Probing the cathepsin D using a BODIPY FL-pepstatin A: applications in fluorescence polarization and microscopy. J. Biochem. Biophys. Methods. 42:137–151. https://doi.org/10.1016/S0165-022X(00)00048-8

Diehl, J.A., F. Zindy, and C.J. Sherr. 1997. Inhibition of cyclin D1 phosphorylation on threonine-286 prevents its rapid degradation via the ubiquitin-proteasome pathway. Genes Dev. 11:957–972. https://doi.org/10.1101/gad.11.8.957

Diehl, J.A., M. Cheng, M.F. Roussel, and C.J. Sherr. 1998. Glycogen synthase kinase-3beta regulates cyclin D1 proteolysis and subcellular localization. Genes Dev. 12:3499–3511. https://doi.org/10.1101/gad.12.22.3499

Efeyan, A., W.C. Comb, and D.M. Sabatini. 2015. Nutrient-sensing mechanisms and pathways. Nature. 517:302–310. https://doi.org/10.1038/nature14190

Ferguson, S.M.. 2015. Beyond indigestion: emerging roles for lysosome-based signaling in human disease. Curr. Opin. Cell Biol. 35:59–68. https://doi.org/10.1016/j.ceb.2015.04.014

Galluzzi, L., F. Pietrocola, J.M. Bravo-San Pedro, R.K. Amaravadi, E.H. Baehrecke, F. Cecconi, P. Codogno, J. Debnath, D.A. Gewirtz, V. Karantza, et al. 2015. Autophagy in malignant transformation and cancer progression. EMBO J. 34:856–880. https://doi.org/10.15252/embj.201490784

Goel, S., M.J. DeCristo, S.S. McAllister, and J.J. Zhao. 2018. CDK4/6 Inhibition in Cancer: Beyond Cell Cycle Arrest. Trends Cell Biol. 28:911–925. https://doi.org/10.1016/j.tcb.2018.07.002

Hsu, C.L., E.X. Lee, K.L. Gordon, E.A. Paz, W.C. Shen, K. Ohnishi, J. Meisenhelder, T. Hunter, and A.R. La Spada. 2018. MAP4K3 mediates amino acid-dependent regulation of autophagy via phosphorylation of TFEB. Nat. Commun. 9:942. https://doi.org/10.1038/s41467-018-03340-7

Jansen, V.M., N.E. Bhola, J.A. Bauer, L. Formisano, K.M. Lee, K.E. Hutchinson, A.K. Witkiewicz, P.D. Moore, M.V. Estrada, V. Sánchez, et al. 2017. Kinome-Wide RNA Interference Screen Reveals a Role for PDK1 in Acquired Resistance to CDK4/6 Inhibition in ER-Positive Breast Cancer. Cancer Res. 77:2488–2499. https://doi.org/10.1158/0008-5472.CAN-16-2653

Koff, A., A. Giordano, D. Desai, K. Yamashita, J.W. Harper, S. Elledge, T. Nishimoto, D.O. Morgan, B.R. Franza, and J.M. Roberts. 1992. Formation and activation of a cyclin E-cdk2 complex during the G1 phase of the human cell cycle. Science. 257:1689–1694. https://doi.org/10.1126/science.1388288

Latré de Laté, P., A. Pépin, H. Assaf-Vandecasteele, C. Espinasse, V. Nicolas, M.L. Asselin-Labat, J. Bertoglio, M. Pallardy, and A. Biola-Vidamment. 2010. Glucocorticoid-induced leucine zipper (GILZ) promotes the nuclear exclusion of FOXO3 in a Crm1-dependent manner. J. Biol. Chem. 285:5594–5605. https://doi.org/10.1074/jbc.M109.068346

Li, Y., M. Xu, X. Ding, C. Yan, Z. Song, L. Chen, X. Huang, X. Wang, Y. Jian, G. Tang, et al. 2016. Protein kinase C controls lysosome biogenesis independently of mTORC1. Nat. Cell Biol. 18:1065–1077. https://doi.org/10.1038/ncb3407

Li, L., H.J. Friedrichsen, S. Andrews, S. Picaud, L. Volpon, K. Ngeow, G. Berridge, R. Fischer, K.L.B. Borden, P. Filippakopoulos, et al. 2018. A TFEB nuclear export signal integrates amino acid supply and glucose availability. Nat. Commun. 9:2685. https://doi.org/10.1038/s41467-018-04849-7

Lim, S., and P. Kaldis. 2013. Cdks, cyclins and CKIs: roles beyond cell cycle regulation. Development. 140:3079–3093. https://doi.org/10.1242/dev.091744

Luzio, J.P., P.R. Pryor, and N.A. Bright. 2007. Lysosomes: fusion and function. Nat. Rev. Mol. Cell Biol. 8:622–632. https://doi.org/10.1038/nrm2217

Ma, H.T., and R.Y. Poon. 2011. Synchronization of HeLa cells. In Cell Cycle Synchronization. G. Banfalvi, editor. Springer, New York. 151–161. https://doi.org/10.1007/978-1-61779-182-6_10

Martina, J.A., and R. Puertollano. 2013. Rag GTPases mediate amino acid-dependent recruitment of TFEB and MITF to lysosomes. J. Cell Biol. 200:475–491. https://doi.org/10.1083/jcb.201209135

Martina, J.A., Y. Chen, M. Gucek, and R. Puertollano. 2012. MTORC1 functions as a transcriptional regulator of autophagy by preventing nuclear transport of TFEB. Autophagy. 8:903–914. https://doi.org/10.4161/auto.19653

Martina, J.A., H.I. Diab, L. Lishu, L. Jeong-A, S. Patange, N. Raben, and R. Puertollano. 2014. The nutrient-responsive transcription factor TFE3 promotes autophagy, lysosomal biogenesis, and clearance of cellular debris. Sci. Signal. 7:ra9. https://doi.org/10.1126/scisignal.2004754

Medina, D.L., S. Di Paola, I. Peluso, A. Armani, D. De Stefani, R. Venditti, S. Montefusco, A. Scotto-Rosato, C. Prezioso, A. Forrester, et al. 2015. Lysosomal calcium signalling regulates autophagy through calcineurin and TFEB. Nat. Cell Biol. 17:288–299. https://doi.org/10.1038/ncb3114

Mills, J.C., and P.H. Taghert. 2012. Scaling factors: transcription factors regulating subcellular domains. BioEssays. 34:10–16. https://doi.org/10.1002/bies.201100089

Napolitano, G., A. Esposito, H. Choi, M. Matarese, V. Benedetti, C. Di Malta, J. Monfregola, D.L. Medina, J. Lippincott-Schwartz, and A. Ballabio. 2018. mTOR-dependent phosphorylation controls TFEB nuclear export. Nat. Commun. 9:3312. https://doi.org/10.1038/s41467-018-05862-6

Palmieri, M., R. Pal, H.R. Nelvagal, P. Lotfi, G.R. Stinnett, M.L. Seymour, A. Chaudhury, L. Bajaj, V.V. Bondar, L. Bremner, et al. 2017. mTORC1-independent TFEB activation via Akt inhibition promotes cellular clearance in neurodegenerative storage diseases. *Nat. Commun.* 8:14338. https://doi.org/10.1038/ncomms14338

Puertollano, R., S.M. Ferguson, J. Brugarolas, and A. Ballabio. 2018. The complex relationship between TFEB transcription factor phosphorylation and subcellular localization. *EMBO J.* 37. e98804. https://doi.org/10.15252/embj.201798804

Qie, S., and J.A. Diehl. 2016. Cyclin D1, cancer progression, and opportunities in cancer treatment. *J. Mol. Med. (Berl.).* 94:1313–1326. https://doi.org/10.1007/s00109-016-1475-3

Raben, N., and R. Puertollano. 2016. TFEB and TFE3: Linking Lysosomes to Cellular Adaptation to Stress. *Annu. Rev. Cell Dev. Biol.* 32:255–278. https://doi.org/10.1146/annurev-cellbio-111315-125407

Roczniak-Ferguson, A., C.S. Petit, F. Froehlich, S. Qian, J. Ky, B. Angarola, T.C. Walther, and S.M. Ferguson. 2012. The transcription factor TFEB links mTORC1 signaling to transcriptional control of lysosome homeostasis. *Sci. Signal.* 5:ra42. https://doi.org/10.1126/scisignal.2002790

Saftig, P., and J. Klumperman. 2009. Lysosome biogenesis and lysosomal membrane proteins: trafficking meets function. *Nat. Rev. Mol. Cell Biol.* 10:623–635. https://doi.org/10.1038/nrm2745

Sardiello, M., M. Palmieri, A. di Ronza, D.L. Medina, M. Valenza, V.A. Gennarino, C. Di Malta, F. Donaudy, V. Embrione, R.S. Polishchuk, et al. 2009. A gene network regulating lysosomal biogenesis and function. *Science.* 325:473–477. https://doi.org/10.1126/science.1174447

Settembre, C., C. Di Malta, V.A. Polito, M. Garcia Arencibia, F. Vetrini, S. Erdin, S.U. Erdin, T. Huynh, D. Medina, P. Colella, et al. 2011. TFEB links autophagy to lysosomal biogenesis. *Science.* 332:1429–1433. https://doi.org/10.1126/science.1204592

Settembre, C., R. Zoncu, D.L. Medina, F. Vetrini, S. Erdin, S. Erdin, T. Huynh, M. Ferron, G. Karsenty, M.C. Vellard, et al. 2012. A lysosome-to-nucleus signalling mechanism senses and regulates the lysosome via mTOR and TFEB. *EMBO J.* 31:1095–1108. https://doi.org/10.1038/emboj.2012.32

Settembre, C., A. Fraldi, D.L. Medina, and A. Ballabio. 2013. Signals from the lysosome: a control centre for cellular clearance and energy metabolism. *Nat. Rev. Mol. Cell Biol.* 14:283–296. https://doi.org/10.1038/nrm3565

Sherr, C.J., D. Beach, and G.I. Shapiro. 2016. Targeting CDK4 and CDK6: From Discovery to Therapy. *Cancer Discov.* 6:353–367. https://doi.org/10.1158/2159-8290.CD-15-0894

Valenzuela, C.A., L. Vargas, V. Martinez, S. Bravo, and N.E. Brown. 2017. Palbociclib-induced autophagy and senescence in gastric cancer cells. *Exp. Cell Res.* 360:390–396. https://doi.org/10.1016/j.yexcr.2017.09.031

Van Noorden, C.J., E. Boonacker, E.R. Bissell, A.J. Meijer, J. van Marle, and R.E. Smith. 1997. Ala-Pro-cresyl violet, a synthetic fluorogenic substrate for the analysis of kinetic parameters of dipeptidyl peptidase IV (CD26) in individual living rat hepatocytes. *Anal. Biochem.* 252:71–77. https://doi.org/10.1006/abio.1997.2312

Vega-Rubin-de-Celis, S., S. Peña-Llopis, M. Konda, and J. Brugarolas. 2017. Multistep regulation of TFEB by MTORC1. *Autophagy.* 13:464–472. https://doi.org/10.1080/15548627.2016.1271514

Vijayaraghavan, S., C. Karakas, I. Doostan, X. Chen, T. Bui, M. Yi, A.S. Raghavendra, Y. Zhao, S.I. Bashour, N.K. Ibrahim, et al. 2017. CDK4/6 and autophagy inhibitors synergistically induce senescence in Rb positive cytoplasmic cyclin E negative cancers. *Nat. Commun.* 8:15916. https://doi.org/10.1038/ncomms15916

Wang, W., Q. Gao, M. Yang, X. Zhang, L. Yu, M. Lawas, X. Li, M. Bryant-Genevier, N.T. Southall, J. Marugan, et al. 2015. Up-regulation of lysosomal TRPML1 channels is essential for lysosomal adaptation to nutrient starvation. *Proc. Natl. Acad. Sci. USA.* 112:E1373–E1381. https://doi.org/10.1073/pnas.1419669112

Xu, H., and D. Ren. 2015. Lysosomal physiology. *Annu. Rev. Physiol.* 77:57–80. https://doi.org/10.1146/annurev-physiol-021014-071649

Yang, C., and X. Wang. 2017. Cell biology in China: Focusing on the lysosome. *Traffic.* 18:348–357. https://doi.org/10.1111/tra.12483

Zhang, M., B. Hu, T. Li, Y. Peng, J. Guan, S. Lai, and X. Zheng. 2012. A CRM1-dependent nuclear export signal controls nucleocytoplasmic translocation of HSCARG, which regulates NF-κB activity. *Traffic.* 13:790–799. https://doi.org/10.1111/j.1600-0854.2012.01346.x
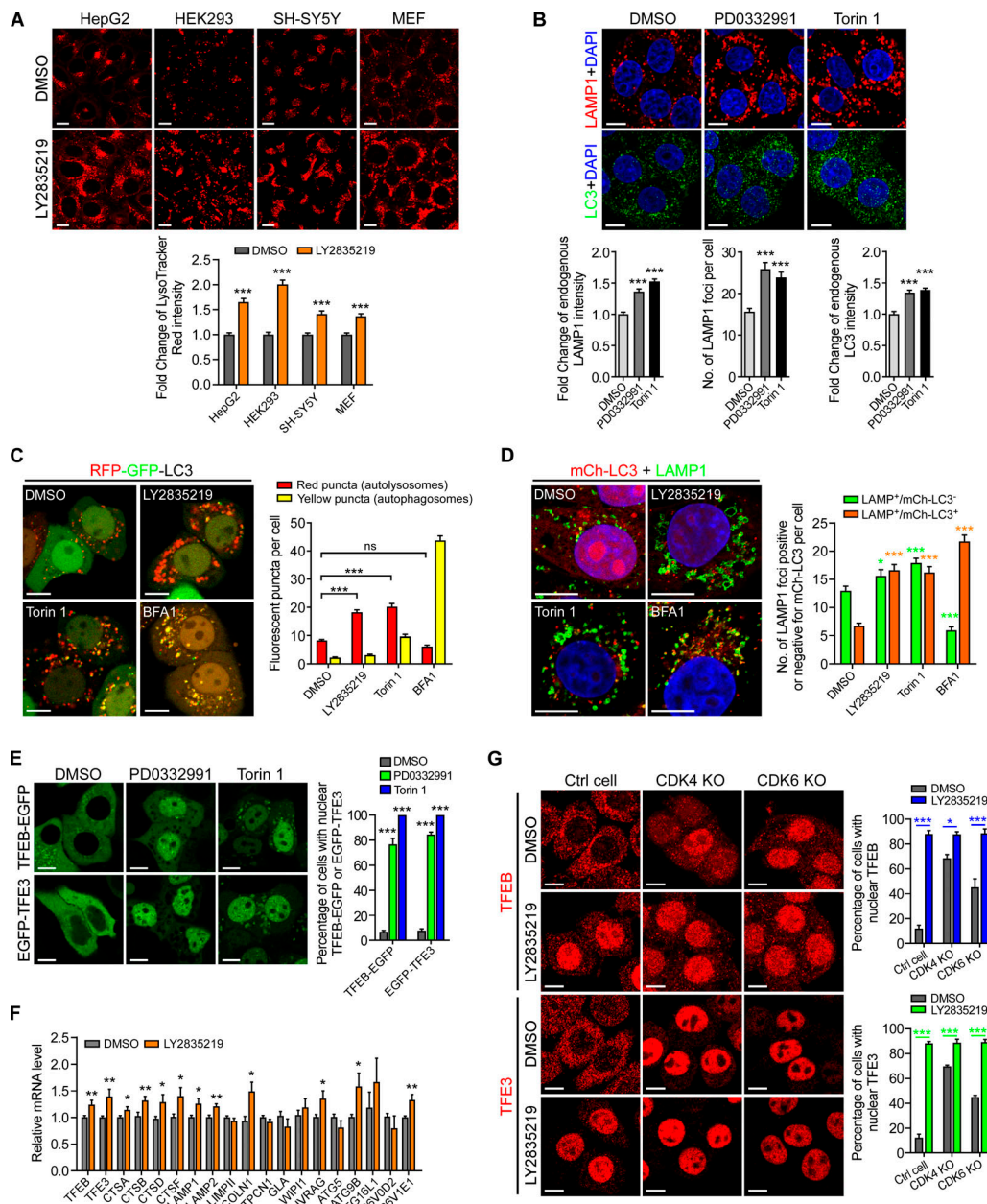
Supplemental material

Figure S1. **CDK4/6 inhibitors induce lysosome biogenesis. (A)** LY2835219 promotes lysosome biogenesis in multiple cell lines. HepG2, HEK293, SH-SY5Y, and mouse embryonic fibroblast (MEF) cells were treated with LY2835219 (2.5 µM, 3 h) and stained with LysoTracker Red. Representative images (upper) and quantification (lower, fold change of LysoTracker Red staining) of lysosomes are shown. ≥35 cells were quantified for each treatment. **(B)** PD0332991 enhances lysosome biogenesis and autophagic levels. HeLa cells were treated with PD0332991 (5 µM, 3 h) or Torin 1 (1 µM, 3 h) and immunostained with LAMP1 and LC3B. Images (upper) and quantification (lower) of lysosome levels (fold change of LAMP1 intensity and number of LAMP foci) and autophagic level (fold change of LC3B intensity) are shown. ≥30 cells were quantified for each treatment. **(C)** Images (left) of RFP-GFP-LC3 in HeLa cells treated with LY2835219 (1 µM), Torin 1 (1 µM), or BFA1 (0.4 µM) for 6 h. Quantification (right) of autolysosomes (red puncta) and autophagosomes (yellow puncta) in cells is shown on the left. ≥60 cells were quantified in each group. **(D)** HeLa cells expressing mCherry-LC3 (mCh-LC3) were treated with LY2835219 (1 µM), Torin 1 (1 µM), or BFA1 (0.4 µM) for 6 h and immunostained with LAMP1 antibody. Images (left) and quantification (right) of the number of lysosomes (LAMP1) that are positive or negative for mCh-LC3. Comparisons are made between DMSO and treatment with LY2835219, Torin 1, or BFA1 within the same color group. ≥30 cells were quantified in each group. **(E)** PD0332991 induces nuclear localization of TFEB-EGFP and EGFP-TFE3. HeLa cells expressing TFEB-EGFP or EGFP-TFE3 were treated with PD0332991 (5 µM, 3 h) or Torin 1 (1 µM, 3 h). Representative images (left) and quantification (right) of the percentage of cells with nuclear TFEB-EGFP or EGFP-TFE3 are shown. Comparisons are made between DMSO and treatment with LY2835219 or Torin 1. ≥400 cells were quantified in each group. **(F)** LY2835219 up-regulates the expression of TFEB-targeted genes. HeLa cells were treated with LY2835219 (1 µM, 3 h), and qRT-PCR analyses were performed. **(G)** Images (left) and quantification (right) of the subcellular localization of endogenous TFEB and TFE3 in control (Ctrl), CDK4 KO, and CDK6 KO cells treated with DMSO or LY2835219 (1 µM, 3 h). Comparisons are made between DMSO and treatment with LY2835219 within the same cell line. ≥300 cells were quantified in each group. Scale bars represent 10 µm in all images. For all quantifications, data (mean ± SEM) were from three independent experiments and were analyzed using the unpaired two-tailed t test or one-way ANOVA with the post hoc Holm-Sidak test. *, P < 0.05; **, P < 0.01; ***, P < 0.001. ns, not significant.
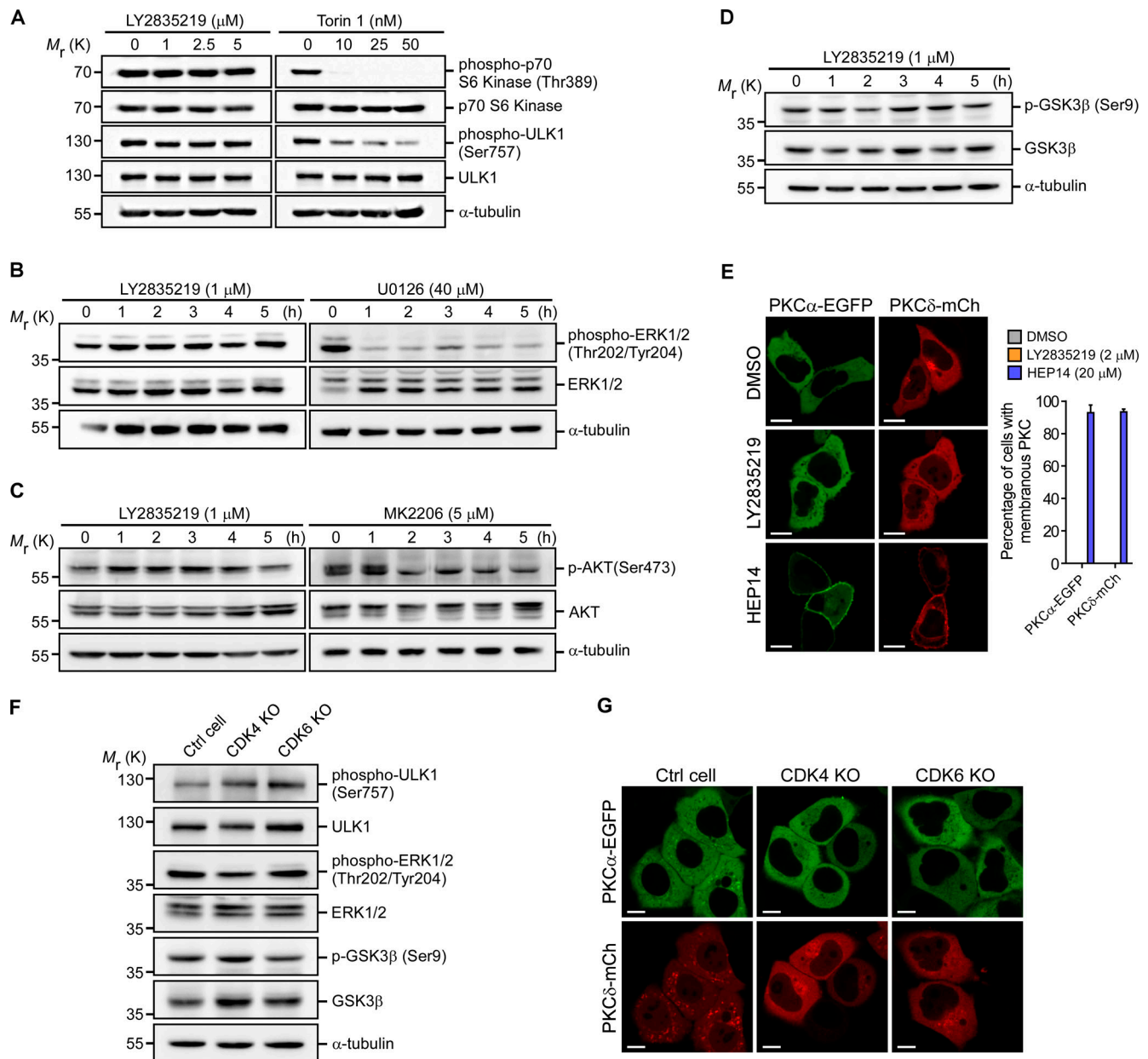
Figure S2. **Inactivation of CDK4/6 has no direct effect on mTOR, ERK2, AKT, GSK3β, and PKC activities. (A)** Immunoblot analysis of the levels of phosphorylated S6K and ULK1 in HeLa cells treated with LY2835219 (left) or Torin 1 (right). Cells were harvested after 3-h treatment and subjected to Western blot analysis. **(B)** Immunoblot analysis of the level of phosphorylated ERK2 in HeLa cells treated with LY2835219 (1 µM, left) or ERK inhibitor U0126 (40 µM, right) for the indicated times. **(C)** Immunoblot analysis of the level of phosphorylated AKT in HeLa cells treated with LY2835219 (1 µM, left) or AKT inhibitor MK2206 (5 µM, right) for the indicated times. **(D)** Immunoblot analysis of the level of phosphorylated GSK3β in HeLa cells treated with LY2835219 (1 µM) for the indicated times. **(E)** Representative images (left) and quantification (right) of PKCα-EGFP and PKCδ-mCherry (PKCδ-mCh) localizations in HeLa cells treated with LY2835219 (2 µM, 3 h) or HEP14 (20 µM, 3 h). ≥200 cells were quantified in each group. **(F)** mTOR, ERK2, and GSK3β activities are not affected in CDK4 KO and CDK6 KO cells. Immunoblotting of ULK1 p-Ser757, ERK1/2 p-Thr202/Tyr204, and GSK3β p-Ser9 was performed in CDK4 and CDK6 KO cells. **(G)** Subcellular localization of PKCα-EGFP and PKCδ-mCh in control, CDK4 KO, and CDK6 KO cells. Images shown are representative of three independent experiments. Scale bars represent 10 µm in E and G.
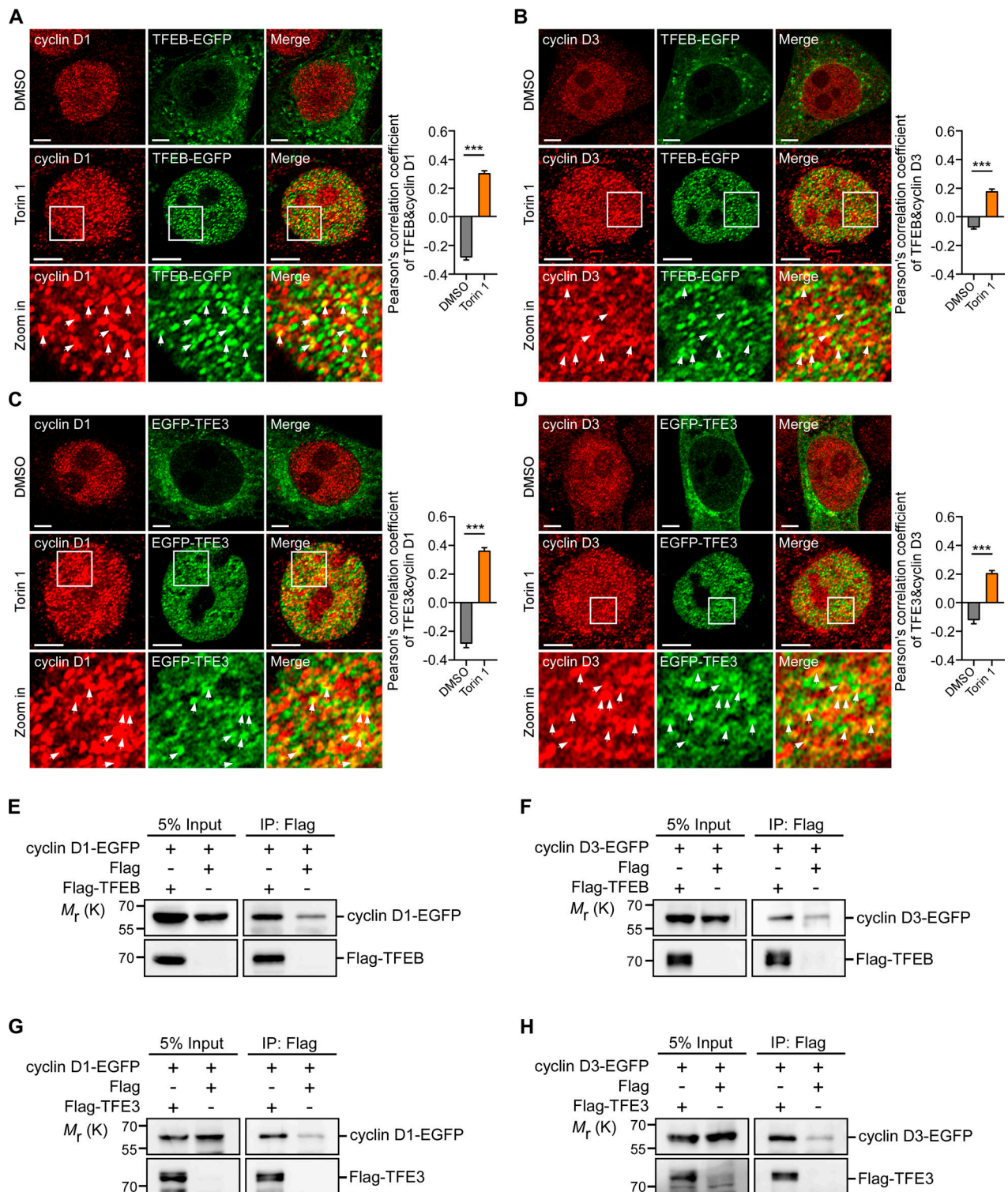
Figure S3. **Cyclin D1 and cyclin D3 interact with TFEB and TFE3. (A and B)** Colocalization of TFEB-EGFP with endogenous cyclin D1 (A) and cyclin D3 (B). HeLa cells transfected with TFEB-EGFP were treated with Torin 1 (1 µM, 3 h), fixed, and stained with cyclin D1 or cyclin D3 antibodies. Framed regions in the middle row are magnified and shown at the bottom. Arrowheads indicate the colocalized proteins. Quantification of the protein colocalization is shown in the right panels. **(C and D)** Colocalization of EGFP-TFE3 with endogenous cyclin D1 (C) and cyclin D3 (D). HeLa cells transfected with EGFP-TFE3 were treated with Torin 1 (1 µM, 3 h), fixed, and stained with cyclin D1 or cyclin D3 antibodies. Framed regions in the middle row are magnified and shown at the bottom. Arrowheads indicate the colocalized proteins. Quantification of the protein colocalization is shown in the right panels. **(E and F)** Co-IP of Flag-TFEB with cyclin D1–EGFP (E) and cyclin D3–EGFP (F). IPs were performed with Flag antibody, and precipitated proteins were detected with antibodies against Flag or EGFP. **(G and H)** Co-IP of Flag-TFE3 with cyclin D1–EGFP (G) and cyclin D3–EGFP (H). IPs were performed with Flag antibody, and precipitated proteins were detected with antibodies against Flag or EGFP. Scale bars represent 5 µm in all images. For all quantifications, data (mean ± SEM) were from three independent experiments and were analyzed using the unpaired two-tailed t test. ≥30 cells were quantified for each treatment. ***, P < 0.001.
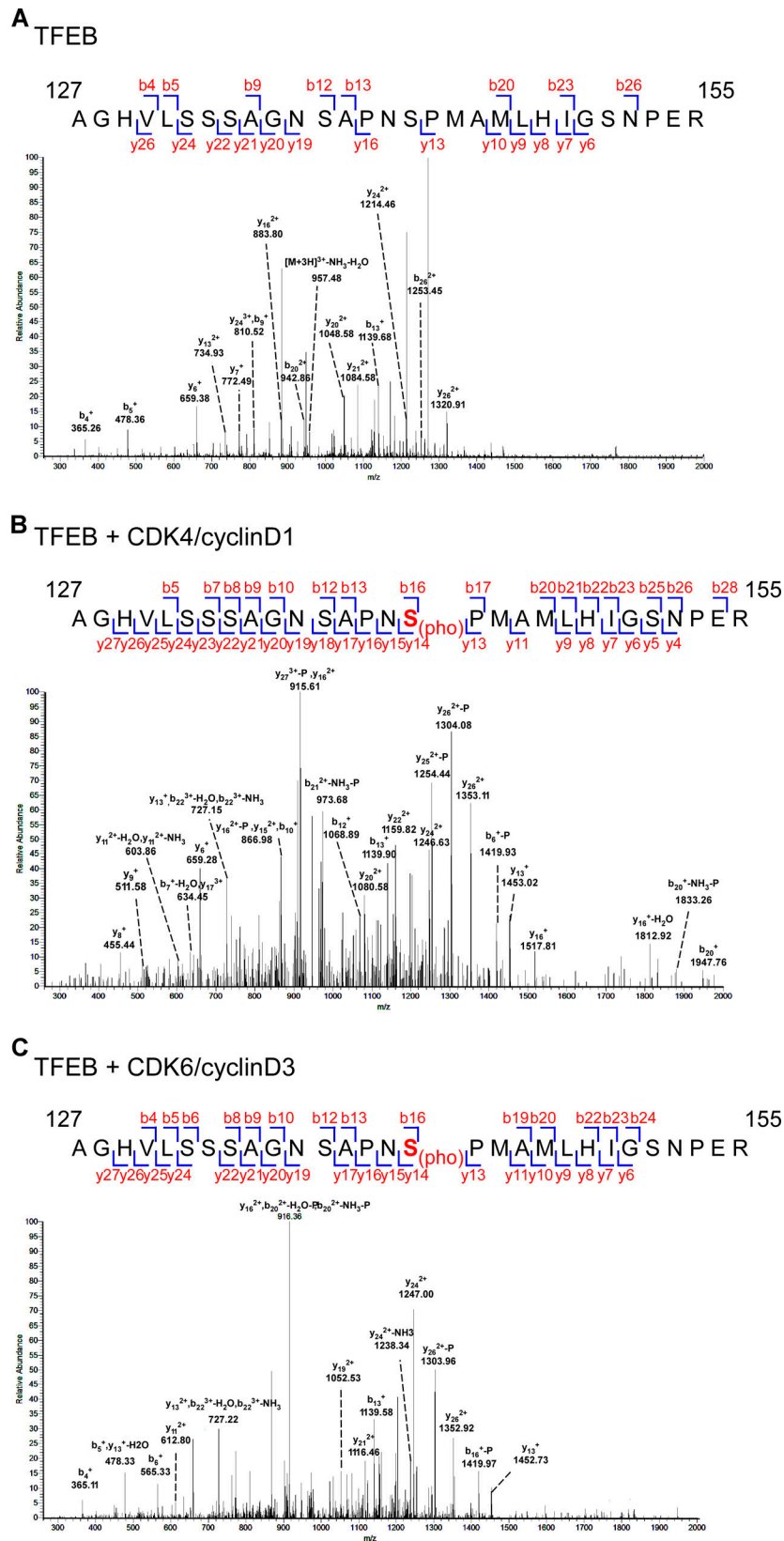
Figure S4. **Mass spectrometry analysis of the phosphorylated sites in TFEB(105–300) after treatment with CDK4/cyclin D1 or CDK6/cyclin D3 complex. (A)** Mass spectrometry analysis of the phosphorylation at Ser142 of TFEB(105–300) with no kinase. **(B)** Mass spectrometry analysis of the phosphorylation at Ser142 of TFEB(105–300) treated with CDK4/cyclin D1 complex. **(C)** Mass spectrometry analysis of the phosphorylation at Ser142 of TFEB(105–300) treated with CDK6/cyclin D3 complex. Peptide ions containing Ser142 with no phosphorylation (A) and with phosphorylation (pho; B and C) are indicated in red.
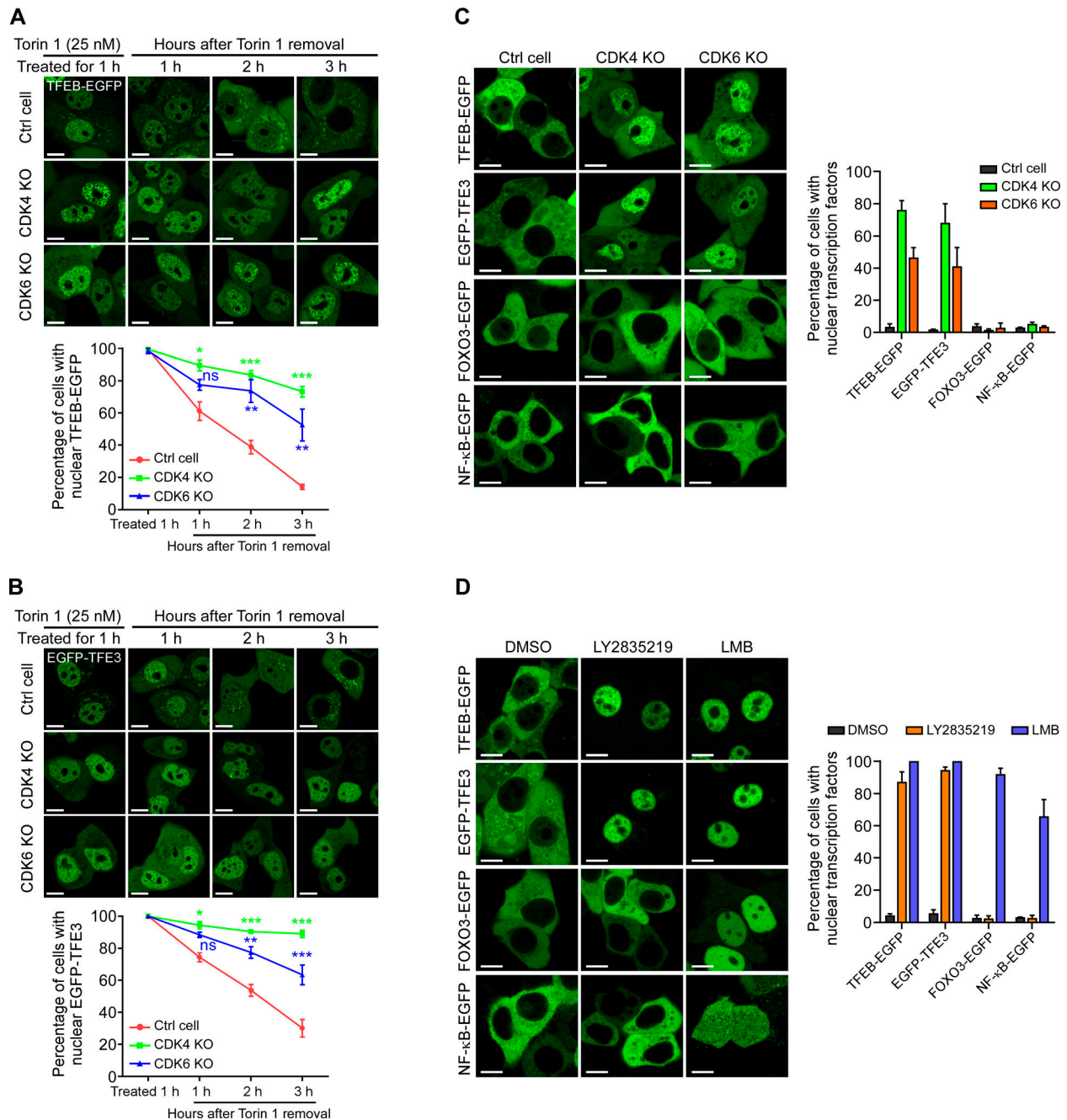
Figure S5. **CDK4 and CDK6 are essential for TFEB and TFE3 nuclear export. (A and B)** Control (Ctrl), CDK4 KO, and CDK6 KO HeLa cells expressing TFEB-EGFP or EGFP-TFE3 were treated with Torin 1 (25 nM, 1 h) and further cultured in fresh DMEM medium to observe the subcellular localization of TFEB-EGFP (A) or EGFP-TFE3 (B) at the indicated time points. Representative images (upper) and quantification (lower) of nuclear localized TFEB-EGFP or EGFP-TFE3 at each time point are shown. ≥300 cells were quantified in each treatment. **(C)** Images (left) of the subcellular localization of TFEB-EGFP, EGFP-TFE3, FOXO3-EGFP, or NF-κB–EGFP in Ctrl, CDK4 KO, and CDK6 KO cells. Quantification (right) of the cells with nuclear localized transcription factors in Ctrl, CDK4 KO, and CDK6 KO cells. ≥200 cells were quantified in each treatment. **(D)** HeLa cells expressing TFEB-EGFP, EGFP-TFE3, FOXO3-EGFP, or NF-κB–EGFP were treated with LY2835219 (1 µM, 3 h), Torin 1 (1 µM, 3 h), and LMB (20 nM, 3 h). Images (left) and quantification (right) of the cells with nuclear localized transcription factors are shown. ≥200 cells were quantified in each treatment. Scale bars represent 10 µm in all images. For all quantifications, data (mean ± SEM) were from three independent experiments and were analyzed using one-way ANOVA with the post hoc Holm-Sidak test. Comparisons are between control cells and KO cells. *, P < 0.05; **, P < 0.01; ***, P < 0.001. ns, not significant.

Tables S1–S7 are provided online as separate Excel tables. Table S1 shows the effects of other CDK inhibitors on TFEB translocation. Table S2 lists the chemical compounds and reagents used in the study. Table S3 contains the siRNA oligos. Table S4 lists the antibodies used in the study. Table S5 lists the expression vectors used in this study. Table S6 contains the oligos for site-directed mutagenesis. Table S7 lists the primers for qRT-PCR.

Yin et al.
Lysosome biogenesis in the cell cycle

Journal of Cell Biology   S6
https://doi.org/10.1083/jcb.201911036